Geophysical Monograph 55

THE INFLUENCE OF NORTH PACIFIC ATMOSPHERIC CIRCULATION ON STREAMFLOW IN THE WEST

Daniel R. Cayan

Scripps Institution of Oceanography, A-024,
University of California-San Diego, La Jolla, CA 92093-0224

David H. Peterson

U.S. Geological Survey, MS-496, 345 Middlefield Road,
Menlo Park, CA 94025

Abstract. The annual cycle and nonseasonal variability of streamflow over western North America and Hawaii is studied in terms of atmospheric forcing elements. This study uses several decades of monthly average streamflow beginning as early as the late 1800's over a network of 38 stations. In addition to a strong annual cycle in mean streamflow and its variance at most of the stations, there is also a distinct annual cycle in the autocorrelation of anomalies that is related to the interplay between the annual cycles of temperature and precipitation. Of particular importance to these lag effects is the well-known role of water stored as snow pack, which controls the delay between peak precipitation and peak flow and also introduces persistence into the nonseasonal streamflow anomalies, with time scales from 1 month to over 1 year.

The degree to which streamflow is related to winter atmospheric circulation over the North Pacific and western North America is tested using correlations with time averaged, gridded sea level pressure (SLP), which begins in 1899. Streamflow fluctuations show significant large-scale correlations for the winter (December through February) mean SLP anomaly patterns over the North Pacific with maximum correlations ranging from 0.3 to about 0.6. For streams along the west coast corridor the circulation pattern associated with positive streamflow anomalies is low pressure centered off the coast to the west or northwest, indicative of increased winter storms and an anomalous westerly-to-southwesterly wind component. For streams in the interior positive streamflow anomalies are associated with a positive SLP anomaly stationed remotely over the central North Pacific, and with negative but generally weaker SLP anomalies locally.

One important influence on streamflow variability is the strength of the Aleutian Low in winter. This is represented by the familiar Pacific-North America (PNA) index and also by an index defined herein the "CNP" (Central North Pacific). This index, beginning in 1899, is taken to be the average of the SLP anomaly south of the Aleutians and the western Gulf of Alaska. Correlations between PNA or CNP and regional anomalies reflect streamflow the alternations in strength and position of the mean North Pacific storm track entering North America as well as shifts in the trade winds over the subtropical North Pacific. Regions whose streamflow is best tuned to the PNA or CNP include coastal Alaska, the northwestern United States, and Hawaii; the latter two regions have the opposite sign anomaly as the former. The pattern of streamflow variations associated with El Niño is similar, but the El Niño signal also includes a tendency for greater than normal streamflow in the southwestern United States. These indices are significantly correlated with streamflow at one to two seasons in advance of the December-August period, which may allow modestly skillful forecasts. It is important to note that streamflow variability in some areas, such as British Columbia and California, does not respond consistently to these broad scale Pacific atmospheric circulation indices, but is related to regional atmospheric anomaly features over the eastern North Pacific.

Spatially, streamflow anomalies are fairly well correlated over scales of several hundred kilometers. Inspection of the spatial anomalies of streamflow in this study suggest an asymmetry in the spatial pattern of positive versus negative streamflow anomalies in the western United States: dry patterns have tended to be larger and more spatially coherent than wet patterns.

Introduction

Most of the surface water west of the Continental Divide in North America is supplied by North Pacific air masses [Rasmusson, 1967; Klein and Bloom, 19871. The bulk of this precipitation occurs during the cool season [Hsu and Wallace, 19761 from extratropical storms that are carried in the westerly flow. The seasonal migration of this storm track provides a marked annual cycle and results in a distinct geographical pattern, with precipitation generally decreasing from north to south and from coastal ranges to the interior. This distribution is compounded by topography, which can either enhance the precipitation in a given region or diminish it, depending on its orientation relative to the flow [e.g., Weaver, 1962; Pittock, 1977].

Atmospheric patterns involved in western cool season precipitation are often broad in scale with up and downstream connections, so that systematic deviations in the atmospheric flow over the North Pacific are involved in North American precipitation anomalies. In the central North Pacific the time-mean surface pressure configuration, called the Aleutian-Gulf of Alaska Low, is generally lower during winters with frequent cyclone passages and higher during winters when these cyclone passages are less frequent, less intense, or diverted to another location. Marked year-to-year changes in this activity makes this region the seat of largest monthly and seasonal scale variability in the northern hemisphere [Namias, 19751. The dynamics of the atmospheric flow produce an organized spatial pattern: averages of a

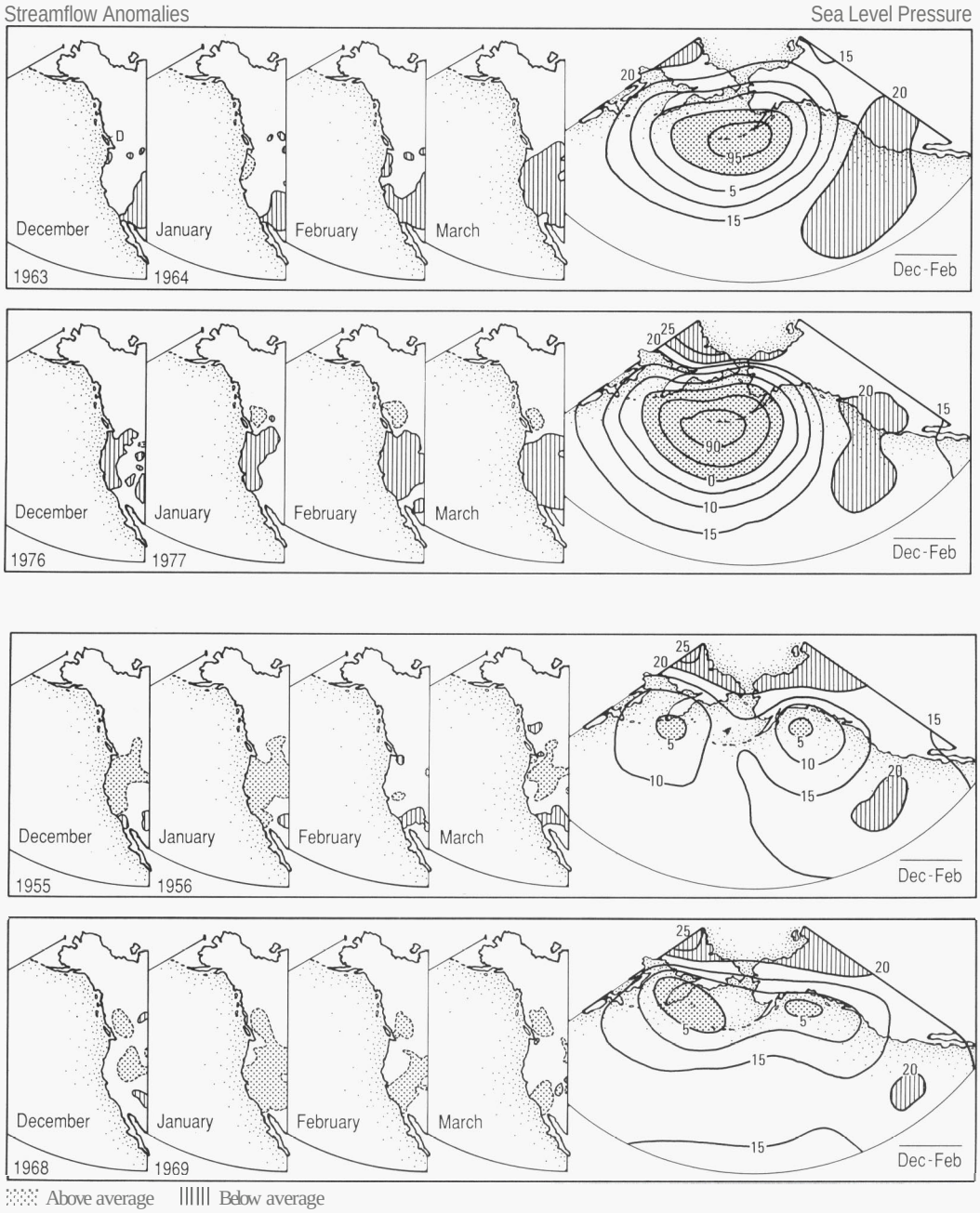

Fig. 1. Streamflow anomaly for December–March and winter mean SLP for pairs of winters (a) 1963–1964 and 1976–1977 and (b) 1955–1956 and 1968–1969 when atmospheric circulation pattern over North Pacific was similar. For anomalies in the upper or lower quartile of a given stream's monthly distribution see Peterson et al. [1987a]. 1000 mb is subtracted from SLP, contour interval is 5 mb.

few days and more show that storm activity around the hemisphere is arranged in cells that correspond to the troughs (or negative anomalies of pressure or geopotential) of atmospheric quasi-stationary planetary waves which usually have dimension of several hundred to thousands of kilometers [see, e.g., Madden, 1979]. This wavy character of the atmospheric flow gives rise to remote correlations of the anomaly patterns called "teleconnections," which are pronounced features of time-averaged circulation [Namias, 1981; Wallace and Gutzler, 1981; Blackmon et al., 1984]. As will be shown this large peak winter atmospheric structure provides a loose organization to the streamflow anomalies that carries through the runoff season.

Many authors have demonstrated how the climatic conditions in North America are related to the circulation far afield over the central North Pacific. In particular the precipitation along the Pacific coast of North America is strongly affected by the orientation of the North Pacific storm track [e.g., Namias, 1978a; Yarnal and Diaz, 1986]. Meteorologists have

struggled to measure, describe, and forecast precipitation; the difficulty has been its spotty spatial make-up and episodic nature that are symptoms of complex governing dynamics. Fortunately, a significant portion of the precipitation variability can be specified from the anomalous time-averaged atmospheric circulation, using regression techniques [Klein, 1963; Walsh et al., 1982; Weare and Hoeschele, 1983; Cayan and Roads, 1984; Klein and Bloom, 1987]. Spatial averaging of the precipitation appears to improve the resultant relations with the circulation ranging over synoptic time scales to monthly and seasonal phenomena. Numerous studies have related the time-averaged atmospheric circulation to precipitation, but very few have examined its linkage to streamflow, possibly because of complications that might be introduced by surface processes such as evapotranspiration. These processes render streamflow to be only a fraction of the precipitation input to a watershed [see, e.g., Court, 1974]. This fraction varies with temperature, soil, and soil cover, and with meteorological properties; values typically range from greater than 70 percent for high latitude tundra regions to less than 3 percent for deserts [Sellers, 1965]. In California runoff totaled over the state is estimated to be 35 percent of the total precipitation input [State of California, 1979]. There are, however, incentives for studying streamflow variability. Streamflow is a more usable form of water than the precipitation, and streamflow represents a natural spatial and temporal average that filters the noisier precipitation field. In addition streamflow samples high elevation, severe topographic regions where direct precipitation measurements are often sparse, and thus is capable of representing the regions where the input of water is often greatest. An interesting issue that underlies this study is the extent to which the atmospheric circulation "signal" can be distinguished in the monthly streamflow variability.

Streamflows have fluctuated considerably over the instrumental record [e.g., Roden, 1967; Langbein and Slack, 1982; Bartlein, 1982; Meko and Stockton, 1984] and the socio-economic, physical, and biological significance of this year-to-year variability is great. The impact of this Variability is particularly strong in the western United States, where water resources are limited. While most of the area east of the Mississippi River receives, on average, an excess of 30 inches (76 cm) of precipitation annually, much of the West is limited to considerably less. With the exception of the coastal Northwest, the surficial water supply is largely derived from high elevation precipitation that is distributed in the form of streamflow. A better grasp of how interannual streamflow variability is driven by the climate system is a first step toward prediction and better management of the water supply. Also, to the extent that stream chemistry is flow related, an associated connection with the streamflow variability is the budget of chemical species in rivers affected by interannual fluctuations in flow driven by climate [Peterson, et al., 1987a; Peterson et al., 1987b]. These natural variations need to be understood in order to quantify man-caused effects.

Visual examination of anomalous streamflow maps [Holmes, 1987] suggests that similar streamflow anomaly patterns emerge from similar winter atmospheric circulation over the North Pacific. As an example, the dependence of streamflow on circulation type is demonstrated in Figure 1, showing December–March streamflow anomalies within two pairs of winters, each pair sharing a distinct atmospheric circulation pattern. The remarkable difference between the two pairs of maps suggests a rather strong effect of winter North Pacific atmospheric circulation on streamflow in the West. This study is aimed at demonstrating the link between climate forcing and western streamflow. We shall address the following two issues: (1) What is the seasonal behavior of streamflow anomalies and how is it related to atmospheric elements such as temperature and precipitation? and (2) What is the link between the North Pacific winter atmospheric circulation and the streamflow anomalies over western North America?

The text is arranged as follows: data sets employed are described, the seasonal cycle of streamflow over the domain is discussed, an analysis of the linkage with the large scale winter circulation is presented, foreshadowing of anomalous streamflow from seasonal atmospheric indices is discussed, and a view of some regional scale correlations within the streamflow network is shown.

Data and Data Processing

Data employed in *this* study include monthly and seasonal mean atmospheric and streamflow instrumental records. The streams were selected to provide reliable records over the longest possible period. Monthly average streamflow from 38 stations over western North America and Hawaii were obtained from the U.S. Geological Survey and Canada archive [Department of Interior, 1975]. The 38 streams include 29 from the western conterminous United States, 3 from British Columbia, 4 from Alaska, and 2 from Hawaii. Most of the streamflow records begin between 1900 and the 1930's; the longest series, Spokane River at Spokane, Washington, begins in 1891. The four Alaskan streams have no data until the late 1940's, with the exception of Gold Creek at Juneau, which has a short segment of early data from 1917–1920. Some stream records have a several-year gap; such gaps occur mostly in 1900–1935. However, because we found no obvious inconsistencies of these earlier (pregap) data with the longer and more recent data segments, the pregap data were included in the analysis.

The 38 streams are described with associated statistics in Table 1. The largest river in the set is Fraser River (at Hope, British Columbia), which had a long-term annual mean of 2720 ($m^3 s^{-1}$), and the smallest rivers of the set were Arroyo Seco in southern California at 0.28 ($m^3 s^{-1}$), and Kalihi River in Oahu, Hawaii, at 0.17 ($m^3 s^{-1}$). Most of the North American rivers which drain into the North Pacific Ocean in this set are described by Roden [1967]. Nonseasonal (anomalous) variability changes considerably between these rivers. In relative terms the stream with the smallest variability is Fraser River, a large northern river fed by ample snowmelt, whose annual mean flow ranged between 71 percent and 135 percent of its long-term mean. In contrast Arroyo Seco, a small ephemeral stream in southern California occasionally pulsed by floods, ranged from 0 percent to 628 percent of its long-term mean flow. In general these streams exhibited minimum annual discharges from 20 percent to 60 percent of their long-term mean and maximum annual discharges from 150 percent to 250 percent of their long-term mean. Estimates of the average annual flow per unit area for the watersheds, obtained by dividing the mean annual discharge by the total area of the drainage basin, are also presented in Table 1 to directly compare the runoff with the annual precipitation. These annual flow per unit area values are highest for the northern coastal streams with values from 200 cm yr^{-1} to over 350 cm yr^{-1} and lowest in the interior Southwest with values as low as 1 cm yr^{-1}.

In this study the primary data representing the atmospheric circulation is seasonal mean sea level pressure (SLP) over the North Pacific and western North America. Although upper level geopotential fields, such as the 700 millibar (mb) height, are often employed in diagnostic studies of the atmospheric circulation [e.g., Klein and Bloom, 1987; Namias, 1978a], we used SLP. Sea level pressure has a long record length, beginning in 1899, while commonly used geopotential fields do not begin until after World War II in about 1947. Sea level pressure has been shown to be an adequate indicator of atmospheric circulation, especially over the extratopical oceans during winter [Davis, 1978; Emery and Hamilton, 1985] and is reasonably well correlated with precipitation over the west coast [Cayan and Roads, 1984]. Numerous studies have demonstrated the usefulness of monthly and seasonal means as a representation of the collective anomalous synoptic scale events that comprise a given period [e.g., Namias, 1978a, Davis, 1978]. Monthly average SLP for the period 1899 through 1974, documented by Trenberth and Paolino, [1980] was obtained from the National Center for Atmospheric Research. It was updated from data archived at Scripps Institution of Oceanography obtained from the National Meteorological Center from 1975 through 1985. Questions have been raised about the veracity of parts of the SLP data during the earlier period, but these mainly concern the region over Asia and the higher latitudes north of 55 °N. [Trenberth and Paolino, 1980; Jones, 1987]. Sea level pressure data were not available for December 1944 and were missing for scattered grid points across the North Pacific during other months. Seasonal means were constructed by averaging the three appropriate months. Winter is defined as the average of December, January, and February, and so on for the other seasons.

TABLE 1. Description of Streams and Associated Statistics

Stream	Station Number	Area of Drainage (sq km)	Period of Record	Average Annual Mean Flow ($m^3 s^{-1}$)	Average Annual Mean Flow Per Unit Area (cm yr^{-1})	Standard Deviation of Mean Annual Flow ($m^3 s^{-1}$)	Coefficient of Variation from Annual Means	Autocorrelation Averaged Over 1–12 Month Lag	Estimated Time Between Independent Samples (months)	Linear Trend Over Period of Record* ($m^3 s^{-1}$)
Chena River, Fairbanks, AK	15514000	5,127.9	1948–1985	39.1	24.0	13.8	0.35	0.36	3	−12.3
Susitna River, Palmer, AK	15290000	160.3	1948–1985	5.9	116.2	1.4	0.24	0.22	5	0.1
Kenai River, Cooper Landing, AK	15258000	1,642.1	1947–1985	80.9	155.4	15.4	0.19	0.29	4	20.3
Gold Creek, Juneau, AK	15050000	25.3	1917–1982	3.0	371.0	0.4	0.13	0.18	6	0.1
Skeena River at USK, BC	08EF001	42,217.0	1928–1984	907.5	67.8	122.7	0.14	0.18	8	61.2
Fraser River, Hope, BC	08MF005	202,797.0	1912–1984	2,720.8	42.3	363.2	0.13	0.29	10	246.7
Sproat River, Alberni, BC	08HB008	347.1	1913–1984	37.8	343.2	7.2	0.19	0.13	3	0.1
Skagit River, Mt. Vernon, WA	12200500	8,010.9	1940–1985	473.5	186.4	79.1	0.17	0.25	7	48.7
Skykomish River, Gold Bar, WA	12134500	1,385.7	1928–1985	112.4	255.7	24.6	0.22	0.19	3	13.3
Spokane River, Spokane, WA	12422500	11,111.1	1891–1985	194.4	55.2	51.0	0.26	0.27	10	−8.6
Clark Fork, St. Regis, MT	12354500	27,736.3	1910–1985	215.4	24.5	60.1	0.27	0.40	18	16.1
Clearwater River, Spalding, ID	13342500	24,786.3	1910–1986	438.3	55.8	105.6	0.24	0.22	3	68.8
Yakima River, Kiona, WA	12510500	14,542.9	1905–1985	104.4	22.6	32.2	0.31	0.24	7	−3.2
Chehalis River, Grand Mound, WA	12027500	2,318.1	1928–1985	81.1	110.4	18.8	0.23	0.15	1	11.8
Wilson River, Tillamook, OR	14301500	417.0	1914–1985	34.3	259.2	7.1	0.21	0.14	1	−3.2
Willamette River, Salem, OR	14191000	18,855.2	1909–1985	663.8	111.0	138.6	0.21	0.22	8	143.2
Umpqua River, Elkton, OR	14321000	9,539.0	1905–1985	214.8	71.0	53.6	0.25	0.25	11	22.0
John Day River, Service Creek, OR	14046500	13,183.1	1929–1985	55.5	13.3	22.3	0.40	0.31	12	32.4

Snake River, Weiser, ID.....	13269000	179,228.0	1910–1986	525.4	9.2	150.5	0.29	0.46	17	70.2
Snake River, Heise, ID.....	13037500	14,897.7	1910–1986	198.1	41.9	40.0	0.20	0.36	12	14.3
Weber River, Oakley, UT...	10128500	422.2	1904–1984	6.2	46.7	1.8	0.29	0.44	20	−1.5
Yampa River, Steamboat Springs, CO....	09239500	1,564.4	1904–1985	13.3	26.9	3.8	0.29	0.35	8	−0.8
Animas River, Durango, CO.....	09361500	1,792.3	1897–1985	23.3	41.0	7.8	0.33	0.36	10	−7.2
Green River, Green River, UT.....	09315000	105,154.0	1894–1985	180.2	5.4	61.0	0.34	0.43	21	−56.6
Humboldt River, Palisade, NV.....	10322500	12,975.9	1901–1986	11.4	2.8	8.4	0.74	0.46	14	8.3
Smith River, Crescent City, CA.....	11532500	1,577.3	1931–1985	110.9	221.8	27.2	0.24	0.16	2	27.6
Sacramento River, Verona, CA.....	11425500	55,040.1	1929–1985	555.9	31.9	209.2	0.38	0.38	7	273.0
Cosumnes River, Michigan Bar, CA.....	11335000	1,388.2	1907–1985	14.5	32.8	9.2	0.63	0.41	8	4.3
Walker River, Coleville, CA.....	10296000	466.2	1938–1985	7.5	50.9	3.0	0.40	0.39	7	1.8
Merced River, Happy Isle Bridge, Yosemite, CA.....	11264500	468.8	1915–1985	10.0	67.5	4.0	0.40	0.33	6	2.8
Kings River, AB NF Trimmer, CA.....	11213500	2,465.7	1927–1982	40.7	52.1	19.1	0.47	0.31	3	0.5
Virgin River, Littlefield, AZ.....	09415000	13,183.1	1929–1986	6.9	1.7	3.9	0.57	0.26	10	1.1
Arroyo Seco, Pasadena, CA.....	11098000	41.4	1911–1985	0.3	21.3	0.4	1.28	0.35	14	0.1
Salt River, Roosevelt, AZ....	09498500	11,152.5	1913–1985	25.4	7.2	17.1	0.67	0.22	6	−2.9
Gila River, Safford Valley, Soloman, AZ.....	09448500	20,450.6	1932–1985	12.1	1.9	9.6	0.79	0.21	3	11.3
San Pedro River Charleston, AZ.....	09471000	3,157.2	1904–1985	1.7	1.7	1.0	0.59	0.18	3	−1.2
Wailua River, Lihue, Kauai, HI.....	16068000	16.2	1912–1985	1.3	262.1	0.4	0.29	0.15	1	−0.00
Kalihi Stream, Honolulu, Oahu, HI.....	16229000	6.8	1913–1985	0.2	81.1	0.1	0.50	0.18	3	−0.1

*Linear trend is expressed as differences in trend line, ending-beginning. Values can be divided by number of years of record to obtain trend in $m^3\ s^{-1}\ yr^{-1}$.

Regional average precipitation data for the conterminous United States and Alaska river basins was obtained from the National Oceanographic and Atmospheric Administration (NOAA) divisional monthly average data set [e.g., Karl and Knight, 1985; Cayan et al., 1986] for 1895 through 1985 for divisions in the conterminous United states and from 1931 through 1982 for Alaska [Diaz, 1980]. Representative monthly precipitation for the three Canadian streams was constructed by averaging selected stations with long precipitation records extracted from the National Center for Atmospheric Research monthly mean surface data set. No precipitation analyses were carried out for the two Hawaiian streams because regional average precipitation and temperature data were not conveniently available for the Hawaiian stream basins, and because of concern that precipitation at single stations might be corrupted by local effects such as topography.

Because precipitation and streamflow observations often deviate from a normal distribution, they are sometimes transformed to minimize these non-normal effects [e.g. Klein and Bloom, 1987]. Also, because instrumental records may have picked up a non-natural component because of man-caused effects, they are sometimes treated by removing part of their low frequency content (e.g., by removing the linear trend [Namias, 1978b]). To guard against drawing improper conclusions that might have arisen from either of these properties, the analyses herein were carried out on two versions of the streamflow time series. One version was first detrended by removing each month's linear trend individually, then log transformed, and then "anomalized" by removing long-term monthly means of the resultant series. The second version was the original monthly data with only monthly means subtracted but no trends removed and with no transformations. Comparison of the two sets of analyses yielded similar results, suggesting that the trend removal and the log transformation were not necessary. Inspection of the monthly trends showed them to be relatively small for most of the stations included. The Sacramento River at Verona shows a rather large increasing trend, but this is thought to result from the fortuitous timing with the record starting at the beginning of a prolonged dry spell from the late 1920's to the mid-1930's and the record ending just after a remarkably wet period in the early 1980's. Furthermore, many of the analyses employ the time-averaged anomalies of December–August streamflow, a 9-month period that has considerably less skewness than the series from an individual month. For these reasons nearly all of the analyses shown here are those that used the original nontreated data.

To study anomalous behavior in this system the annual cycle of each of the variables was removed by subtracting the long-term monthly mean. For streamflow the entire length of record was used to construct the long-term mean. This period ranged from 36 to 96 years for the 38 streams. A careful account of precautions necessary for interpreting streamflow records is presented by Roden [1967]. For SLP and the precipitation, the 40-year period from 1946–1985 was taken as the climatological base. To investigate the winter circulation influence on the resulting streamflow, the December–August (winter through summer) total streamflow is employed for several of the analyses. This period accounts for the bulk of the streamflow in the basins considered here, since western streams typically undergo a low flow interlude in fall. For most of the streams the average December–August streamflow was 80 percent or more of the annual mean flow; overall it ranged between 67 percent (Gold Creek, Alaska) and 96 percent (Cosumnes, Merced, and Kings Rivers). This seasonality is apparent in Figure 2 showing histories of streamflow through the 12 months for each year at Umpqua River in coastal Oregon, John Day River in interior Oregon, and Weber River in northern Utah. These three rivers, representing low, moderate, and high elevation watersheds, are also used to illustrate various properties of the streamflow in the following section. Average elevations of the three watersheds are 756 m, 1341 m, and 2771 m, respectively.

Many of the analyses are carried out on the streamflow, in the form of cross-correlations and composites. An idea of the anomaly structure for several of the streams is provided by the time series of the standardized

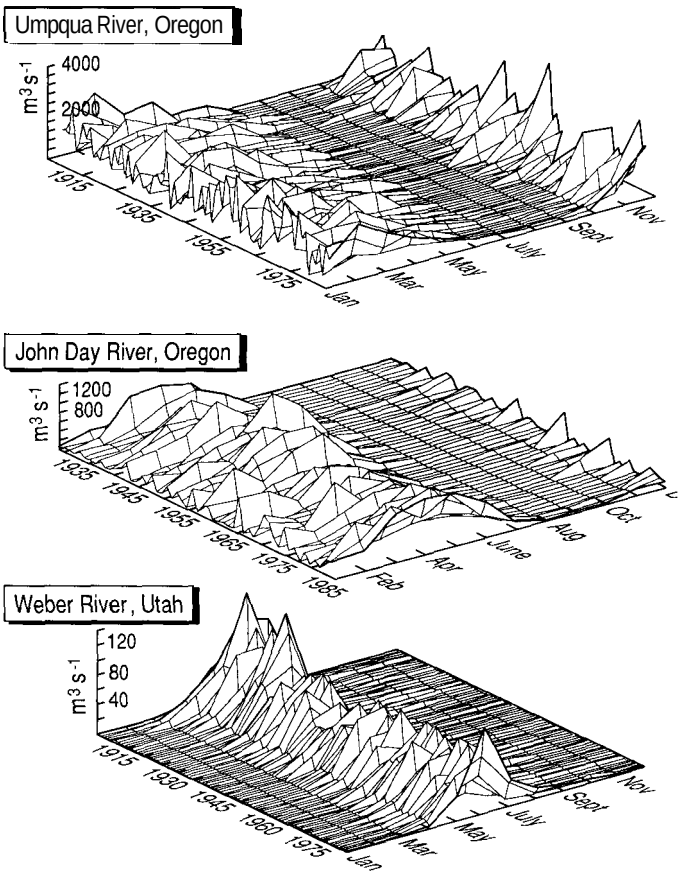

Fig. 2. Time history of monthly streamflow for Umpqua, John Day, and Weber Rivers. Months and years as indicated. Mean annual and monthly streamflow values are presented in Tables 1 and 2, respectively.

anomalies in Figure 3. The statistical significance of the cross-correlation and compositing analyses carried out in this study depends on the number of independent samples in the streamflow time series. The number of independent samples is less than the number of months of observations because of autocorrelation in the streamflow. The time between independent samples was estimated by integrating the autocorrelation function [Leith, 19731. This integral time scale is only a rough approximation, owing to the limited record length of the sample and because the autocorrelation structure varies with season for most streams. In this case the autocorrelation and the resultant integral time scale shown in Table 1 were computed from the detrended log transformed streamflow anomalies. For the 38 stations considered this integral time scale ranged from 1 to 21 months (Table 1). For most of the stations the integral time scale was 1 year or less. For 6 stations, it was greater than 12 months, and for 17 stations, it was 6 months or less. With the above cautions in mind, we diminish the effective length of record when applying traditional tests as a gauge of the significance of the correlation coefficients. For example, given a record for 1930–1985 (56 winter seasons) having 18 months between independent samples (37 independent samples), then correlation coefficients with absolute values in excess of 0.3 are significant at the 95 percent confidence level. Thus in the analyses that follow, the 0.3 level is used throughout as a coarse threshold of significant correlations.

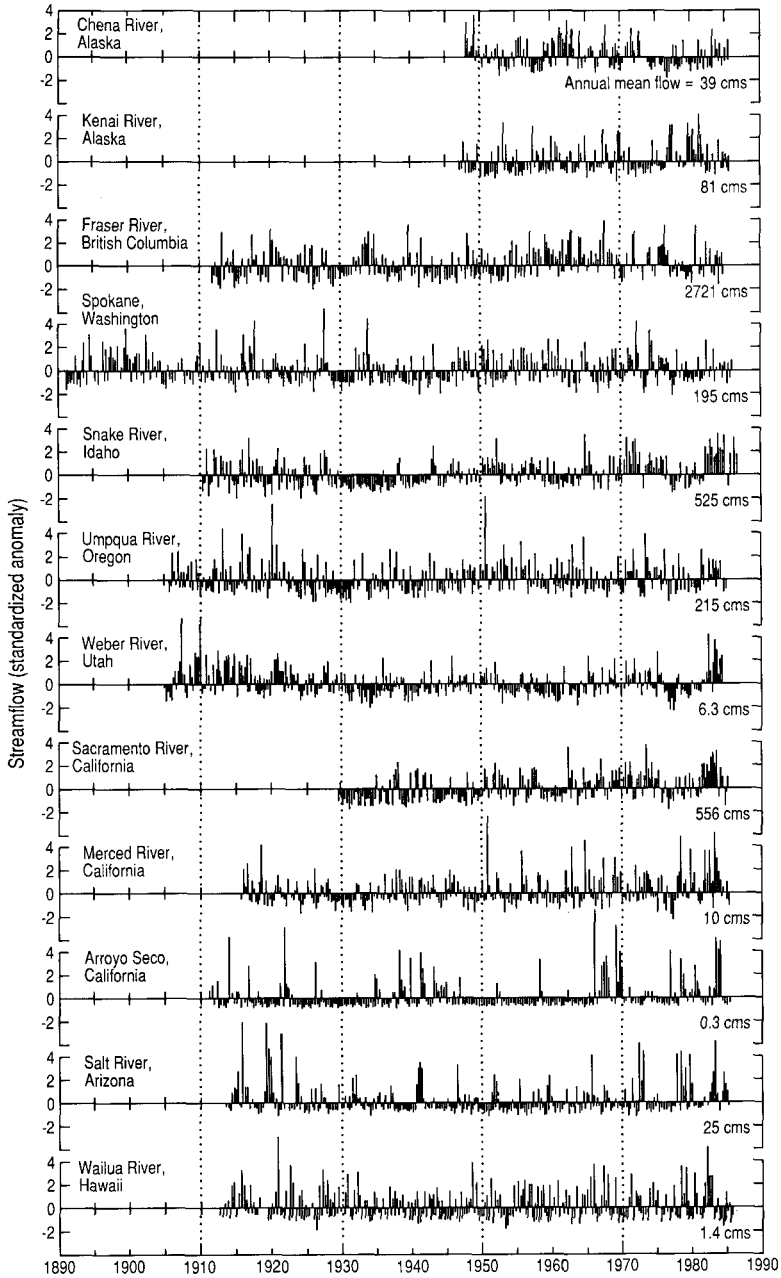

Fig. 3. Time series of monthly streamflow anomalies for selected stations. Anomalies are standardized by dividing by standard deviation for each month. Long-term mean annual streamflow ($m^3 s^{-1}$) is noted for each series.

Streamflow "Climatology"

Most of the streams in this network exhibit a strong seasonal variation in mean streamflow, which follows the climate forcing elements such as precipitation and temperature. In fact, the annual cycle is such a prominent feature of hydrology in the west that it permeates the statistical character of anomalies as well as the mean fields. Comparison of the annual cycle among various basins provides insight into the physical factors affecting their streamflow properties.

The mean annual cycle of streamflow and precipitation is represented in Figure 4 by the amplitude and phase of its first harmonic (periodic at 12 months), patterned after a similar analysis of global precipitation by Hsu and Wallace [1976]. Very simply, this analysis presents each basin's annual harmonic (having a period of 12 months) of precipitation and streamflow

using an arrow, whose length is proportional to the amplitude of the cycle and whose direction indicates its phase. The amplitude and phase are obtained by fitting a 12-month sine wave to the long-term monthly means divided by the annual average of the 12 monthly means. In this rendition the amplitude is the ratio of variance of the fitted annual harmonic divided by the actual variance of the monthly means about the annual average. Thus stations with amplitudes close to 1 have much of their climatological variability in the annual cycle, while those with small amplitudes require other harmonics for a good description. The direction of the arrows point to the month when the annual harmonic has its maximum (positive) value. For example, a station whose annual harmonic is maximum in January points up, as denoted by the dial on the figure. For the mean precipitation, represented by the dashed arrows of Figure 4, the annual harmonic is prominent along the west coast, with amplitudes ranging between 0.4 and 0.9. The annual harmonic of precipitation is not very strong at several basins

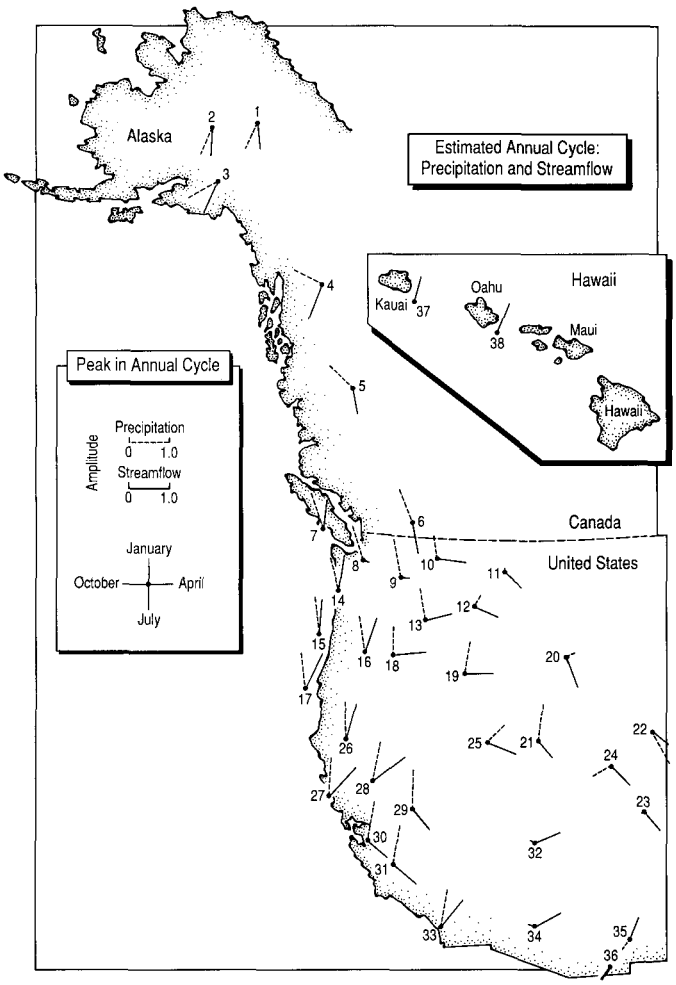

Fig. 4. Normalized amplitude and phase of the annual cycle of monthly precipitation (dotted arrows) and streamflow (solid arrows). Normalized amplitude indicated by length of the arrows, given by scale. Phase is given by direction of arrow (an arrow pointing up indicates maximum in January, one pointing to the right indicates maximum in April, etc.). Station numbers refer to numbering of stations in Table 1.

in the interior western United States, particularly those in Arizona, Colorado, Idaho, and Montana with amplitudes less than 0.4. The timing of maximum precipitation through the year varies considerably over the region as shown by the direction of the dashed arrows [see also Pyke, 1972; Hsu and Wallace, 1976]. Maximum precipitation occurs in summer in the three northern Alaskan basins, in fall in southern Alaska and central British Columbia, in early-to-late winter along the west coast, and varies between spring, summer and fall in the interior western United States. This analysis does not include precipitation for the two Hawaiian stream basins, but Lyons [1982] reported that most Hawaiian rainfall stations have a modest annual cycle of precipitation that peaks in northern hemisphere winter. Turning to the streamflow, represented by the solid arrows in Figure 4, the annual harmonic ranges from 0.2 to almost 1.0 over most of the basins. Several streams have an annual harmonic that is somewhat stronger than that of the precipitation, probably owing to the influence of temperature through the snow storage and melting process. The phase lag between mean streamflow and precipitation is readily seen in this figure, with streamflow lagging by 0 to several months. This delay is greatest in northern and high elevation basins with an appreciable snowpack. Virtually all of these streams exhibit a maximum in the annual harmonic between midwinter and late summer.

For comparison with the harmonic analysis the observed phase lag can be seen from monthly mean precipitation and streamflow in the Umpqua, John Day, and Weber Rivers in Figure 5. Mean precipitation for both coastal and interior Oregon is maximum in December, but while the streamflow lags by only about 1 month along the coast at Umpqua River, it lags by about 4 months at John Day River. The Weber River region has a broad precipitation maximum in winter, but the cold temperatures in this high elevation watershed produce a sharply delayed streamflow peak in May–June (see also Figure 2). Similar plots show that basins in the north and in the interior have peak streamflow which lags one-to-several months after maximum precipitation, apparently because of the snowpack. On the other hand basins along the southern coast and those in Hawaii and southern Arizona are too warm for storage of precipitation in the form of snow, and they exhibit a nearly immediate response (0–1 month) of the streamflow to precipitation. These variations in the lag between precipitation and runoff is well known to hydrologists and also depends on other physical characteristics of a watershed. Analyses of the basins included here confirm that the delay increases as the temperature decreases, which is in many cases affected by increased elevation. In addition to pervading the annual cycle the expected delay between precipitation and streamflow is apparent in the anomaly structure of streamflow, as demonstrated below through the autocorrelation.

Besides the mean the higher order streamflow statistics also exhibit a discernible annual variation, as illustrated by the standard deviation and the 1-month autocorrelation at Umpqua, John Day, and Weber Rivers (Figure 5), and listed for several other "representative" stations (Table 2). For most basins the variance (standard deviation) of these two streams is highest in months having greatest mean streamflow. To compare the variance between stations and within the year the coefficient of variation, defined as the ratio of the standard deviation to the mean, was also computed. This coefficient is smallest for large northern streams, such as Fraser River, showing values of 0.2 and 0.4 and is highest for small streams such as Salt River, showing values of 0.7 to 2.0. Several streams have a maximum coefficient of variation just before or just after peak flow, implying that year-to-year fluctuations in timing of the rise or fall in flow is an important factor in determining the relative amount of streamflow variance. In addition to showing monthly statistics, Table 2 also shows some analogous statistics calculated from annual streamflow values. Because higher frequency monthly variations are diminished when the annual mean is computed, the coefficient of variation of the annual means is smaller than that reflecting monthly data, ranging from 0.13 at Fraser River to 1.32 at Arroyo Seco. In California these annual values are somewhat higher than values derived

for cool season precipitation, which typically range from 0.3 to 0.5 [Granger, 1977]. The skewness of monthly streamflow is usually positive, as it is for precipitation. Its pattern over the year is more variable than the lower order moments, as the skewness can be dominated by relatively few extreme high streamflow events. Skewness is relatively high during months that have generally consistent streamflow except for occasional extreme flood events. Geographically, drier areas to the south that are irregularly punctuated by floods have high skewness, such as at San Pedro River (mean annual runoff per unit area 1.2 cm yr^{-1}) in southern Arizona. The high skewness in Southwest streams mainly results from late summer thunderstorms and tropical storm activity and early winter frontal systems or cutoff lows (D. Meko, R. Webb and J. Betancourt, personal communications) that occur infrequently enough to yield heavy runoff during months when it is normally light. Skewness is low for streams with a high base flow that are not marked by floods. This is typical of wetter areas to the north which have high mean precipitation and relatively smaller anomalous variability, such as Skykomish River (mean annual runoff per unit area 252 cm yr^{-1}) in the Pacific Northwest.

The relatively high persistence of streamflow distinguishes it from precipitation and makes it a potentially valuable index of short period climate variability. The persistence of streamflow anomalies, represented by the autocorrelation, exhibits a marked annual variation at most basins and displays several climatic influences. An understanding of the autocorrelation behavior can be derived from a nonstationary streamflow model, such as by Moss and Bryson [1974], where the flow in a river during a given period is the result of two kinds of components: (1) direct runoff and base flow from within-period precipitation occurring in the basin and (2) water released from storage of pre-period precipitation in the basin. Since precipitation anomalies have little persistence on monthly and longer time scales (autocorrelations of monthly precipitation at 1- and 2-month lags have values less than 0.25 for nearly all pairs of months at several climatological divisions that were examined), most of the month-to-month persistence of streamflow anomalies results from releases into the river from storage that have time scales of a month or longer. The Moss and Bryson [1974] model considers these releases to be in the form of ground water that percolated into a stream, but in the basins considered here, a major portion of storage must arise from snow and ice. The persistence strengthens both as the steadiness of releases from storage and as the importance of storage releases relative to the direct precipitation. In several basins the precipitation minimum during the late spring through summer coincides with and follows the period of maximum streamflow. Consequently, if late spring streamflow is higher than normal, then the subsequent flow in the summer months still tends to remain higher because this flow is virtually all drawn from stored water. Similarly, negative anomalies tend to persist from lower-than-normal spring flows. Thus the components of this system can be thought of as "signal" and "noise" in a prediction scheme, whose skill is indicated by the autocorrelation of anomalous streamflow. The unsteady, atypical releases from storage, such as (1) an unusually early spring melt due to anomalously high temperatures and (2) the direct precipitation components of streamflow in the target month, act as noise. Steady releases from storage, such as the normal seasonal melting of the winter snowpack, is the signal, and the autocorrelation is high during months when (on average) this signal is high relative to the unsteady component.

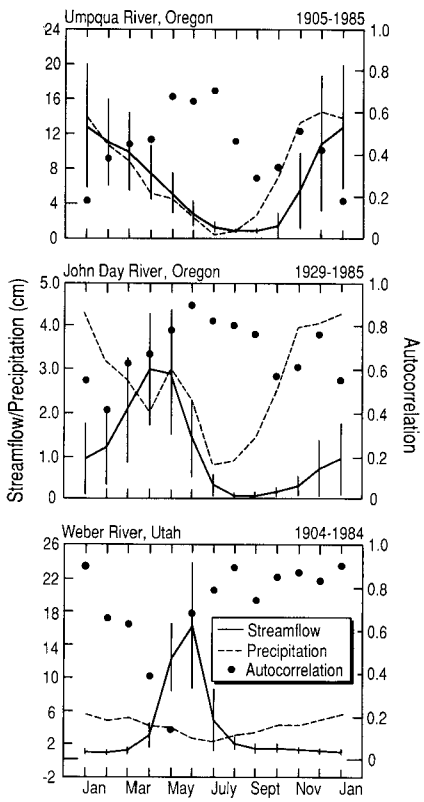

Fig. 5. Monthly long-term mean "streamflow" (solid line), standard deviation of monthly "streamflow" (bars), 1-month lag autocorrelation of streamflow anomalies (•), and monthly long-term mean precipitation (dotted line) for Umpqua, John Day, and Weber Rivers. Streamflow has been divided by the area of the watershed to make mean and standard deviation units comparable to precipitation. One-month lag autocorrelation plotted under leading month, e.g., the one labeled "January" is for January to February, etc.

The seasonal structure of the anomaly persistence can be clearly seen from the 1-month lag autocorrelation and mean monthly flow at Umpqua, John Day, and Weber Rivers in Figure 5. All three rivers have a minimum in autocorrelation during the period when mean flow is rising. The autocorrelation is sensitive to the characteristics of each basin, seen by the shift in timing from winter to late spring as peak precipitation and peak runoff shifts. Umpqua River, the coastal low elevation basin with little snowpack and thus little storage, has a January–February dip in 1-month lag autocorrelation when nonpersistent, high variance precipitation input to the stream is greatest. This is confirmed by the cross-correlations between precipitation and streamflow during winter months (not shown) which are generally greater than 0.7 at Umpqua. Further inland, the higher elevation John Day watershed shows the effect of snowmelt, with an April–May peak in runoff and a pronounced autocorrelation minimum in February–March when precipitation is still high and streamflow is rising sharply. Cross-correlations between John Day streamflow and both precipitation and temperature (not shown) are both positive during this period of the year. Finally, Weber River, fed by high elevation Rocky Mountain snowmelt, has peak streamflow in June and a sharp dip in autocorrelation in April–May, when streamflow is rising rapidly. Cross-correlations of Weber River streamflow and temperature (not shown) are positive and relatively high (0.3 to 0.5) during late spring, again supporting the interpretation that streamflow is significantly affected by either temperature hastening or delaying the snowmelt then. All three basins show high 1-month lag autocorrelations during the period of year after precipitation has fallen off. This reflects the "uncontaminated" influence of the storage of water in the basin. The apparent influence of climate suggested by the progression of the lag structure at these three stations is reinforced from inspection of the autocorrelations of the entire set of streams, which reveals a surprisingly consistent organization according to elevation (temperature) and seasonal mean precipitation.

TABLE 2. Annual Cycle of Various Streamflow Properties at Selected Streams

Stream/Year of Record	January	February	March	April	May	June	July	August	September	October	November	December	Annual*
Kenai River, 1947–1985													
Mean ($m^3 s^{-1}$)	22.1	18.0	14.0	14.2	49.7	148.2	196.2	181.9	147.1	92.6	53.2	31.0	80.9
Standard Deviation ($m^3 s^{-1}$)	13.3	12.4	7.2	6.2	20.5	39.9	34.9	42.6	60.5	45.9	26.6	15.4	15.4
Standard Deviation/Mean	.60	.69	.51	.43	.41	.27	.18	.23	.41	.50	.50	.50	.19
Skewness	2.48	2.01	1.24	1.31	.58	1.03	1.36	1.28	.95	1.67	1.12	1.45	1.63
Maximum/Mean	3.60	3.25	2.26	2.13	1.91	1.91	1.51	1.78	2.21	2.74	2.60	2.65	1.46
Minimum/Mean	.40	.39	.42	.52	.37	.62	.74	.57	.51	.39	.35	.33	.70
Lag 1 Autocorrelation**	.92	.87	.77	.50	.62	.57	.58	.35	.09	.46	.59	.51	.27
Fraser River 1912–1984													
Mean ($m^3 s^{-1}$)	938.0	873.7	836.2	1,671.3	4,868.4	7,029.0	5,625.3	3,604.7	2,446.3	1,983.0	1,582.4	1,138.5	2,720.8
Standard Deviation ($m^3 s^{-1}$)	261.9	250.4	251.8	573.1	1,130.2	1,272.9	1,200.2	790.2	564.7	566.3	498.2	361.8	363.1
Standard Deviation/Mean	.28	.29	.30	.34	.23	.18	.21	.22	.23	.29	.31	.32	.13
Skewness	.90	1.10	1.38	.28	.31	.76	.72	1.23	1.22	.74	.53	.87	.92
Maximum/Mean	1.95	1.85	2.19	2.02	1.68	1.54	1.71	1.79	1.82	1.74	1.79	2.12	1.35
Minimum/Mean	.55	.57	.58	.40	.55	.62	.65	.66	.63	.52	.46	.47	.71
Lag 1 Autocorrelation**	.79	.78	.52	.30	.27	.97	.77	.71	.64	.68	.73	.72	.13
Spokane River, 1891–1985													
Mean ($m^3 s^{-1}$)	158.6	175.1	229.3	403.7	525.7	326.9	101.1	52.6	50.5	60.7	92.9	145.1	194.4
Standard Deviation ($m^3 s^{-1}$)	120.4	101.9	115.5	134.0	176.9	179.6	66.1	21.5	11.8	19.1	50.4	107.5	51.0
Standard Deviation/Mean	.76	.58	.50	.33	.34	.55	.65	.41	.23	.31	.54	.74	.26
Skewness	2.59	1.02	1.28	.17	-.17	.75	1.90	1.66	.89	1.99	2.25	1.87	.97
Maximum/Mean	4.54	2.65	3.13	1.76	1.77	2.59	3.33	2.55	1.85	2.63	3.98	4.47	1.70
Minimum/Mean	.24	.24	.25	.27	.31	.19	.36	.41	.52	.61	.35	.24	.41
Lag 1 Autocorrelation**	.52	.49	.35	.55	.69	.69	.86	.64	.27	.71	.72	.69	.15
Umpqua River, 1905–1985													
Mean ($m^3 s^{-1}$)	454.8	433.9	352.0	275.2	184.9	107.7	49.7	33.5	33.8	54.4	200.7	388.0	214.8
Standard Deviation ($m^3 s^{-1}$)	248.8	192.2	157.0	112.4	81.3	52.0	20.7	6.8	9.5	47.7	158.9	273.6	53.6
Standard Deviation/Mean	.55	.44	.45	.41	.44	.48	.42	.20	.28	.88	.79	.71	.25
Skewness	.35	.40	.64	.59	.98	1.06	2.36	.46	4.05	5.29	1.34	1.57	1.41
Maximum/Mean	2.17	2.14	2.18	2.11	2.42	2.50	2.89	1.58	2.91	7.39	4.16	3.74	1.55
Minimum/Mean	.09	.09	.28	.25	.30	.28	.42	.59	.62	.40	.12	.09	.52
Lag 1 Autocorrelation**	.17	.37	.46	.66	.64	.66	.69	.45	.28	.33	.50	.41	.21

Weber River. 1904–1984													
Mean (m^3 s^{-1})	1.6	1.6	1.9	5.0	19.6	26.5	7.7	3.2	2.3	2.3	2.0	1.7	6.2
Standard Deviation (m^3 s^{-1})	0.3	0.3	0.6	2.3	6.4	12.3	5.9	1.2	0.8	0.8	0.5	0.4	1.8
Standard Deviation/Mean	.20	.19	.30	.47	.33	.46	.77	.38	.36	.34	.25	.23	.29
Skewness	.73	.56	2.70	1.22	.37	.43	3.10	1.01	1.36	1.51	.78	.62	1.49
Maximum/Mean	1.61	1.52	2.75	2.93	1.85	2.32	5.49	2.30	2.43	2.53	1.76	1.72	1.89
Minimum/Mean	.65	.62	.54	.36	.25	.09	.15	.30	.39	.45	.53	.46	.35
Lag 1 Autocorrelation**	.89	.65	.62	.38	.13	.67	.78	**.88**	.73	**.84**	.86	.82	.26
Sacramento River. 1929–1985													
Mean (m^3 s^{-1})	840.9	975.4	913.1	793.6	627.4	390.3	253.9	255.4	292.2	270.2	382.5	631.9	555.9
Standard Deviation. (m^3 s^{-1})	482.4	468.4	401.0	453.7	362.3	229.9	138.6	149.5	144.8	119.0	222.0	**409.9**	209.2
Standard Deviation/Mean	.57	.48	.44	.57	.58	.59	.55	.59	.50	.44	.58	.65	.38
Skewness	.44	.17	.44	.59	.86	1.26	.66	.43	.53	1.16	1.80	1.11	.72
Maximum/Mean	2.15	1.95	2.21	2.22	2.42	2.81	2.74	2.37	2.14	2.61	3.20	2.89	2.16
Minimum/Mean	.26	.23	.21	.21	.14	.14	***.06***	.09	.29	.36	.29	.27	.34
Lag 1 Autocorrelation**	.60	.75	.67	.84	.89	.57	**.94**	.97	.76	.57	.80	.63	.28
Salt River. 1913 –1985													
Mean (m^3 s^{-1})	28.7	38.8	55.6	58.0	30.1	10.5	9.8	17.0	12.9	13.2	10.5	22.6	25.4
Standard Deviation (m^3 s^{-1})	58.6	51.1	55.6	44.7	30.2	8.6	11.3	13.8	9.5	22.7	10.3	36.8	17.5
Standard Deviation/Mean	2.04	1.32	1.00	.77	1.01	.82	1.16	.81	.74	1.73	.99	1.63	.69
Skewness	5.65	2.59	2.22	.86	2.45	1.88	5.87	3.65	1.91	4.56	3.36	2.77	4.41
Maximum/Mean	15.79	6.62	5.29	3.06	5.59	3.67	9.50	6.02	4.07	10.39	5.82	7.92	3.72
Minimum/Mean	.16	.12	.11	.10	.12	.21	.23	.25	.17	.18	.33	.16	.28
Lag 1 Autocorrelation**	.35	.48	.67	.86	.94	.29	.35	.42	.14	.32	.74	.27	.17
Wailua River, 1912–1985													
Mean (m^3 s^{-1})	1.7	1.4	1.6	1.6	1.4	0.9	1.1	1.1	1.0	1.1	1.6	1.7	1.3
Standard Deviation (m^3 s^{-1})	1.5	0.9	1.1	1.0	0.7	0.4	0.4	0.5	0.5	0.6	1.0	1.0	0.4
Standard Deviation/Mean	.89	.70	.70	.61	.54	.44	.37	.44	.52	.50	.59	.59	.27
Skewness	3.80	1.62	2.47	1.35	1.72	1.19	***.64***	1.21	1.52	.79	1.61	.97	2.93
Maximum/Mean	6.57	3.42	4.70	3.00	3.01	2.56	2.07	2.81	2.99	2.34	3.28	2.67	1.95
Minimum/Mean	.25	.21	.19	.17	.19	.40	.32	.28	.31	.30	.28	.21	.51
Lag 1 Autocorrelation**	.31	.17	.37	.42	.44	.34	.46	.51	.49	.29	.43	.30	.05

*Mean. Standard Deviation. Standard Deviation/Mean, Maximum/Mean, Minimum/Mean and autocorrelation are from annual mean (calendar year average) values. Skewness is computed from all individual months.

**Autocorrelation is for given month and following month; e.g., that listed for January is for January versus February. Autocorrelation for annual values is for 1-year lag.

Relation of Streamflow to North Pacific Atmospheric Circulation Patterns

North Pacific Circulation Versus Streamflow

It might be expected that the strongest links to atmospheric circulation would occur during winter when North Pacific storms are most active and anomalous atmospheric variations are greatest. The deepening of the North Pacific Low and the increase in variance of associated variables is indicated by the standard deviation of seasonal SLP in the central North Pacific, whose maximum value south of the Aleutian Islands increases from 2 mb in summer to 6 mb in winter [Namias, 1975]. The effect of winter atmospheric circulation on streamflow is shown in Figures 6 and 7 by maps showing the cross-correlation between the anomaly of December–August (9-month cumulation) streamflow at a given basin and winter SLP across the North Pacific. Since the spatial variation in the standard deviation of SLP is small, the contours on these maps can be qualitatively interpreted as anomalous geostrophic winds with cyclonic or counter clockwise flow around negative centers and anticyclonic or clockwise flow around positive centers [Stidd, 1954]. Very generally, regions of cyclonic flow anomalies are associated with anomalously high precipitation and anticyclonic flow with low precipitation. Inspection of SLP cross-correlations and composite maps from the other seasons shows that winter SLP has the strongest statistical connection to December–August streamflow for virtually all basins considered, but that the SLP anomaly in fall (preceding) and, for some basins, spring (during) also make significant contributions (for brevity, correlations for these other seasons are not shown here). For several basins the SLP anomaly patterns displayed by fall are similar to winter, albeit somewhat weaker, suggesting that the same physical mechanisms operate. For near-coastal low-to-moderate elevation basins in the southern half of the domain there are significant correlation patterns with spring SLP. These are similar to ones found for winter, and also similar to patterns linking atmospheric circulation with precipitation shown by other researchers [e.g. Klein and Bloom, 1987]. This implies that, for these southern lower elevation basins, spring precipitation is an important influence on streamflow, and that it is produced by similar atmospheric circulation anomaly patterns as in winter. However, correlations with spring SLP are weak for several basins in the north and in higher elevations. Since in spring there is non-negligible precipitation throughout western North America, and precipitation is still related to the circulation [e.g. Klein and Bloom, 19871, it is likely that other mechanisms compete to diminish the relation of streamflow with the atmospheric circulation. One competing mechanism is the temperature field, which would likely increase or decrease streamflow independent of precipitation, since temperature and precipitation are only weakly correlated in the Northwest during spring (J. Namias, personal communication); from this we might infer that the circulation patterns associated with temperature anomalies are nearly independent from the ones associated with precipitation anomalies. In support of this interpretation is the observation that the cross-correlation of streamflow with precipitation is weakened and the cross-correlation of streamflow with temperature is positive during spring months for several of the basins. Analyses are not shown for brevity. A multivariate analysis of the circulation, precipitation, temperature, and streamflow is required to better isolate these mechanisms.

There is a remarkably consistent pattern in the north-to-south sequence of coastal basin SLP cross-correlation maps (Figure 6). An anomalous low pressure center to the west or northwest in winter provides heavier precipitation and higher streamflow on the coast, while an anomalous high pressure center there results in reduced precipitation and streamflow. This pattern is consistent with 700-mb height versus precipitation relation for periods of 1 day to 1 month along the west coast during winter noted by Klein and collaborators [Klein, 1963; Klein et al., 1965; Klein and Bloom, 1987]. The synoptic interpretation of the high streamflow phase of this circulation pattern is that it indicates increased storminess that is carried onshore from the northeast Pacific. The enhanced southerly to southwesterly cyclonic flow associated with the anomalous low to the west or northwest represents an aggregrate of weather systems that produce stronger advection of moisture and vorticity as well as increased upslope vertical motion along the west coast mountain topography, which is generally aligned from south to north. The opposite pattern of anomalous high pressure off-shore indicates a lack of storminess, reduced moisture transport, and suppressed upward vertical motion. The north-south sequence of maps from Alaska to southern California clearly indicates the sensitivity of the coastal streamflow to the placement of the low; the anomalous correlation center "migrates" southward along the coast as the basin location is taken from north to south.

Atmospheric patterns favoring high streamflow in the interior basins of the West (shown in the top four maps of Figure 7) differ sharply from those seen in Figure 6 for the coastal basins. Several of the interior basins have highest positive correlations with positive SLP anomalies located remotely

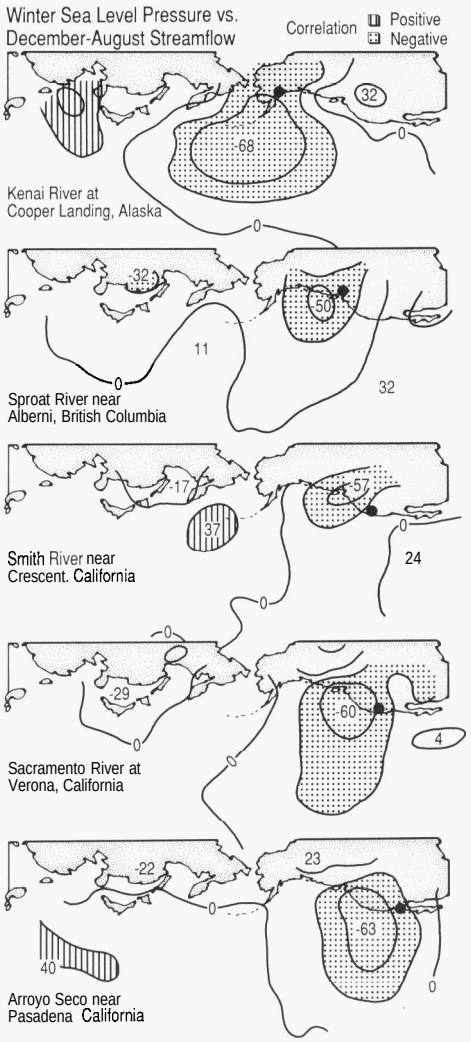

Fig. 6. Cross-correlation between winter North Pacific SLP and December–August streamflow anomalies at five coastal streams (location at dots) from Alaska to Southern California. Correlations are contoured at 0, ± 0.3 and ± 0.5, with shading to indicate magnitude.

to the west and somewhat lower positive correlations with negative SLP anomalies locally. The western positive center is a remote teleconnection rather than a direct regional (low) forcing pattern. This type of pattern is displayed by the northern three basins in Figure 7 (Susitna, Alaska; Clark Fork, Montana; and Weber, Utah). Only the southenunost basin, Salt River, Arizona, shows a winter SLP cross-correlation pattern similar to those of the coastal basins (Figure 6). Correlation with a positive pressure anomaly in the central North Pacific implies both a southerly displaced storm track across the eastern North Pacific and into the West, and probably more activity from storms from Northern Canada and Alaska that drop into the West, east of the Cascades. For Clark Fork and Weber River basins, there are local negative correlations with SLP, but they are relatively small in spatial scale and in magnitude. This result is consistent with Klein et al.'s [1965] observation that in parts of the interior western United States, daily

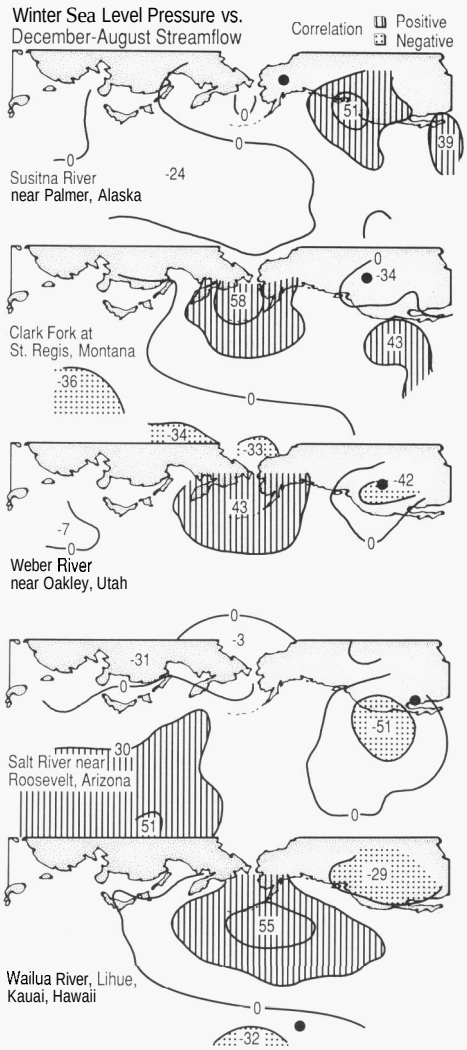

Fig. 7. Cross-correlation between winter SLP over the North Pacific and December–August streamflow anomalies at four interior western North America streams from Alaska to Arizona, plus one stream in the Hawaiian Islands. Correlations are contoured at 0, ± 0.3 and ± 0.5, with shading to indicate magnitude.

precipitation in winter is not favored by southwesterly flow as in the coastal region, but rather by flow with an anomalous northeasterly to southeasterly component. Further, he points out that precipitation in this region is associated with a local trough producing positive vorticity, and not a more remote upstream regime characterized by vorticity advection, as is precipitation in coastal regions. Klein et al. [1965], and Weare and Hoeschele [1983] found, in contrast to the west coast, that in the Rockies and in the Great Basin a smaller fraction of the precipitation variance could be accounted for by upper level geopotential height anomalies. The streamflow-SLP results are consistent with their findings, suggesting that local influences such as topography, surface heating, and friction contribute significantly to the precipitation variability [Cayan and Roads, 1984]. A striking influence of topography can apparently be seen by comparing the SLP relations of the two Alaskan streams, seen in the two top maps of Figure 6 and Figure 7, respectively. Despite the rather close proximity of the two basins (Kenai River drains the northern Kenai Peninsula in the northern Gulf of Alaska and Susitna River drains the Talkeetna Mountains just a few hundred km to the northeast), the links to the circulation are astonishingly different. Increased streamflow in Kenai River results from a deepened Aleutian Low and anomalous southerly winds, while increased streamflow in Susitna River is associated with high SLP centered well to the south but little evidence for a local or regional circulation mechanism. Chena River, which is even farther north and inland of the Alaska Range, displays a correlation to SLP (not shown) which resembles that with Susitna. In fact, the record of streamflow at Chena River has a weak negative correlation with that at Kenai. This contrast appears to be a symptom of Alaska's complex climate, with the fall and winter maritime storms that produce substantial precipitation along the immediate coast, not as apparent in the interior, which is dominated by summer convective precipitation (S. A. Bowling, personal communication). Glacial melt contributing to the flow may also complicate the relation of SLP to streamflow in some of the watersheds

An even larger spatial scale perspective of the influence of circulation on hydrological variability can be seen from the Hawaiian streamflow versus SLP correlations, (bottom panel, Figure 7) in contrast with those for North American streams. The Wailua River, located on the east side of Kauai, Hawaiian Islands, lies in a precipitation regime that is dominated by the interplay between topography and the wind [Solot, 1950]. High streamflow in Wailua River is strongly associated with positive winter SLP anomalies to its north in the central North Pacific and negative SLP anomalies to its southwest. According to Lyons [1982], this SLP configuration yields a most prominent mechanism for precipitation in the Hawaiian Islands: stronger northeasterly trade winds, which produce heavy precipitation on the eastern side of Kauai, due to orographic lifting of the moist subtropical air mass. In contrast high streamflow in Southern California and Arizona is associated with negative anomalous SLP centered to the Northwest or west that indicates strong southwesterly flow, discussed above. Comparison of the Wailua cross-correlation with the one favoring high streamflow in Clark Fork and Weber River in the upper panels reveals a remotely connected similarity; the same winter circulation regimes that result in high or low streamflow in Hawaii tend to result in similar conditions over the northwestern United States. This teleconnection is further illustrated below.

Weak and Strong Winter North Pacific Circulation Versus Streamflow

Cross-correlations discussed above suggest that strong negative SLP anomalies in the central North Pacific produce low streamflow in much of the Northwest and in the Hawaiian streams. Conversely, positive SLP anomalies over the central North Pacific are associated with a circulation that favors high streamflow in these regions.

The well-known PNA index [Horel and Wallace, 1981; Wallace and Gutzler, 1981] is strongly related to anomalous SLP in the central North Pacific, but also includes atmospheric values farther afield over the sub-

tropical North Pacific, western Canada, and southeastern United States. For this study a PNA index [Horel and Wallace, 1981] was constructed from seasonal 700 mb height values over the 1947–1986 period. This version of the PNA is given by

$$\mathrm{PNA} = H(170^\circ\ \mathrm{W.},\ 20^\circ\ \mathrm{N.}) - H(165^\circ\ \mathrm{W.},\ 45^\circ\ \mathrm{N.}) + H(115^\circ\ \mathrm{W.},\ 58^\circ\ \mathrm{N.}) - H(90^\circ\ \mathrm{W.},\ 30^\circ\ \mathrm{N.}) \quad (1)$$

Another phenomenon related to atmospheric circulation over the North Pacific is a prevalence of anomalously deep central North Pacific lows in northern hemisphere winter during the "mature phase" [Rasmusson and Carpenter, 1982] of the El Niño/Southern Oscillation (ENSO) [Bjerknes, 1969; Namias, 1985]. In the available historical record these events have occurred irregularly at an interval of 3–10 years [Quinn and Neal, 1986]. El Niño/Southern Oscillation episodes have accompanied impressive extratropical atmospheric and oceanic anomalies, as the recent 1982–1983 event reminds us [Quiroz, 1983]. The central North Pacific teleconnection is one of the strongest extratropical responses to ENSO [Dickson and Livezey 1984; Namias, 1985]. For the present study the Southern Oscillation Index (SOI), provided by the NOAA Climate Analysis Center, is used as an index for ENSO. It has been noted [Douglas et al., 1982; Esbensen, 1984] that the PNA often, but not always, occurs during ENSO episodes; it can also occur separately.

To further explore the relation of streamflow to atmospheric circulation over the central North Pacific, an SLP index, abbreviated "CNP," was constructed by averaging the SLP over the region 35°–55° N. and 170° E.–150° W. This index is similar to the PNA index, but CNP is available for a longer period than PNA (CNP is available since 1899, while PNA begins in 1947). There are 25 "strong" and 25 "weak" CNP winters, defined as standardized index values greater than or equal to −0.5 and less than or equal to +0.5, respectively (Table 3). To characterize the magnitude of strong and weak CNP cases the average CNP for the 25 strong CNP cases is less than −7 mb, while it exceeds +7 mb for the 25 weak cases. In both of these composites the strongest anomaly center is found at about 50° N., 165° W. It is interesting that these extreme winters tend to cluster in runs, as discussed here later in regard to low frequency variability (also see Ebbesmeyer et al. [this volume] for remarkable low frequency effects on the Puget Sound estuary).

The interrelation among SOI, PNA, and CNP is shown by their seasonal cross-correlations (Table 4). The significant correlations appear to be SOI and PNA during winter and spring, SOI and CNP during winter, and PNA and CNP during winter, spring, and fall. It is also interesting to note that SOI and PNA correlations are of the same magnitude as SOI and CNP correlations for every season except spring. During winter and spring, PNA is significantly (90 percent) correlated ($\rho = -0.41$ and -0.31, respectively) with SOI over 1947–1986. During winter, but not spring, CNP is correlated at about the same magnitude ($\rho = 0.40$ and 0.16, respectively) with SOI albeit with more statistical significance since the 1931–1986 sample size is larger. PNA and CNP are strongly correlated, especially during winter, spring, and fall ($\rho = -.90, -0.75$, and -0.69, respectively). This is somewhat surprising since PNA includes three centers in addition to the central North Pacific region of the CNP. These high correlations indicate the reliability of the teleconnection from the central North Pacific; therefore the great importance of the role of the central North Pacific in forming the PNA. Teleconnection maps of Namias [1981], and Wallace and Gutzler [1981] provide greater details of the PNA structure. We conclude that CNP, formed from the more historically extensive SLP field, is an adequate surrogate for the PNA during winter and fall.

To test the relation of streamflow variability to these atmospheric indices maps of cross-correlations between winter CNP, PNA, and SOI and December–August streamflow anomalies are shown in Figure 8. There is interdependence among these three indices, as indicated by similar spatial patterns in their respective anomaly patterns, their temporal variations, and the resultant correlations with streamflow. As suggested by the individual

TABLE 3. Central North Pacific (CNP) Index: Strong and Weak Winter Cases

[Sea-level pressure (SLP) anomaly averaged over 170° E.–150° W., 35°–55° N.]

Strong		Weak	
Winter*	SLP	Winter*	SLP
	.....	1903	1.3
.....	.....	1907	1.3
	.....	1909	0.9
	.....	1910	1.4
	.....	1911	1.6
1912**	−0.5	1915	1.1
	.....	1916	1.6
	.....	1922	1.2
1926**	−1.4	.....	.....
1927	−0.7	.....	.....
1929	−0.9	.....	.....
1931**	−1.5	.....	.....
	.....	1932	1.5
	.....	1933	0.6
1934	−1.0	.....	.....
1936	−1.6	.....	.....
	.....	1937	2.2
1939	−0.5	.....	.....
1940**	−2.3	.....	.....
1941**	−1.8	.....	.....
1942**	−1.0	.....	.....
	.....	1943	0.6
1944	−0.7	.....	.....
1946	−0.6	.....	.....
	.....	1948	0.8
	.....	1949	1.5
	.....	1950	1.3
	.....	1952	1.0
1953	−1.1		.....
	.....	1955	1.0
	.....	1956	1.4
	.....	1957	0.6
1958**	−0.7		.....
1961	−1.3		.....
1963	−1.4		.....
1964**	−0.7		.....
.....	.....	1966	0.9
.....	.....	1969	1.5
1970**	−1.5		.....
.....	.....	1971	0.7
.....	.....	1972	1.4
1977**	−2.2		
1978	−1.2		.....
.....	.....	1979	1.1
1980	−0.7		
1981	−1.7		.....
.....	.....	1982	0.7
1983**	−1.8		
1986	−1.9		

*Winter is defined such that Winter 1912 is average of (December 1911, January 1912, February 1912).

**Northern hemisphere winter corresponding to El Niño event defined by Quinn et al. [1986] of magnitude greater than or equal to 2.

TABLE 4. Cross-Correlation Between Seasonal SOI, PNA, and CNP Circulation Indices

	SOI and PNA	SOI and CNP	PNA and CNP
Winter	−0.41	0.40	−0.90
Spring	−0.31	0.16	−0.75
Summer	−0.10	0.13	−0.21
Fall	−0.23	0.20	−0.69
Number of Pairs	39	54	39
Two-tailed test value at 95% significance...	10.31|	|0.27|	|0.31|

streamflow versus SLP results (Figure 7), when PNA or CNP indices indicate anomalous low pressure in the central North Pacific, there is a tendency for light streamflow over the northwest coast into the interior from Idaho southward into Utah, light streamflow in the two Hawaiian streams, and high streamflow for stations along the Alaskan coast. The opposite streamflow anomaly scenario is associated with anomalously high pressure in the central North Pacific. However there is almost no correlation between PNA or CNP and streamflow in California, in the Southwest, in British Columbia, and interior Alaska.

The relation of streamflow with strong and weak central North Pacific winter lows can be reconciled using atmospheric teleconnections [Namias, 1981; Wallace and Gutzler, 1981]. Teleconnections (cross-correlations) show that anomalously low 700-mb height in the central North Pacific (centered near 50° N., 170° W.) during winter tends to be accompanied by positive height anomalies over the west coast, as well as positive height anomalies in the subtropical North Pacific; a pattern of anomalies of opposite sign is connected with positive anomalies at this center. Because monthly scale atmosphere features are almost barotropic (anomaly features not vertically tilted) in winter over the extratropical oceans [Wallace and Gutzler, 19811, the interpretation of SLP anomalies is nearly equivalent to the 700-mb anomalies. Inspection of SLP composites (not shown) for strong and weak CNP patterns confirms that the SLP teleconnection pattern is very similar. These teleconnections can be translated in terms of the large scale circulation, the carrying current for North Pacific storms. When the central Pacific low is well developed, North Pacific winter storm tend to be carried northward toward northern British Columbia and Alaska, making that region wet while the northwestern United States is dry. Conversely, when the low is weak, the Gulf of Alaska low to the east is usually active, and the opposite precipitation and streamflow anomaly pattern tends to occur. The mean negative SLP anomalies in the central North Pacific, corresponding to enhanced storminess south of the Aleutian Islands, are associated with a high pressure anomaly ridge downstream over the Northwest, with the storm track routed north into the Alaskan coast instead of into the Pacific coast further south (see Klein [1957] and Reitan [1974] for storm tracks). In the subtropical North Pacific the flow is anomalous westerly (west-to-east) in association with the gradient between the deep central Pacific low to the north and anomalous high pressure to the south. This flow anomaly represents reduced trade winds and an associated diminution of precipitation and streamflow on the eastern coastal slopes of the Hawaiian Islands. The relative weakness of the southern position of the teleconnection center downstream over the west coast means that the tendency for high pressure (lack of storminess) is not very reliable; hence there is not a strong CNP relationship over California and the Southwest.

CNP appears to be a useful index for more than one reason. It is encouraging that for winter the correlations of CNP with streamflow are about the same in magnitude and make a similar spatial pattern as those of PNA with streamflow. This reflects the fact that the pre-1947 (before PNA) relations of streamflow with CNP (not shown) hold up at about the same level as those for the period following. This suggests that these teleconnections and their attendant physical mechanisms are stable features. A second virtue of the CNP is its simplicity of representing the most important winter circulation mode in the central North Pacific, the PNA [Davis 1978; Barnston and Livezey, 1987; Namias et. al., 1988] with regional average SLP anomalies.

The "mature" winter phase [Rasmusson and Carpenter, 1982] of the ENSO is associated with low pressure in the central North Pacific in winter. The SOI versus streamflow anomaly correlation pattern is similar to that of CNP and PNA, but with two differences. In this analysis the SOI correlation along the Alaskan coast is weaker than that with CNP and PNA, although Yarnal and Diaz [1986] reported significant correlations of coastal Alaskan precipitation with ENSO activity. The weakness of this relation probably arises from the variability in the longitude of the North Pacific low, which can be seen from the broad loci of anomalous troughs accompanying strong El Niño during winter (Peterson et al., [1986], Figure 8). A more westerly position of this trough favors the winter storm track moving into the Alaskan coast, while a more easterly position is associated with storms entering the west coast farther south. Further insight into the types of northern hemisphere circulation patterns that appear with ENSO is provided by Fu et. al., [1986], and Livezey and Mo [1987], who suggest that the configuration of tropical Pacific heating may help to determine the pattern of extratropical response.

Interestingly, SOI is significantly related to precipitation and streamflow over the southwestern United States, while PNA and CNP are not. Streamflow anomalies in the Southwest from southern California through Arizona and southern Colorado tend to be positive (wet), while those in the Pacific Northwest are negative (dry) during the warm eastern tropical Pacific phase of ENSO. There is an important distinction between the results with streamflow and the results of a previous investigation of the relation between ENSO and North American precipitation by Ropelewski and Halpert [1986] who found a suggestion that the El Niño phase of ENSO was associated with lighter than average precipitation in the Pacific Northwest, but this tendency was not strong enough for them to consider it to be reliable. Part of the reason for this weakness may be the wavering of timing of the light precipitation between fall and spring. However, in basins with higher elevations streamflow is not as sensitive to these timing changes as is the precipitation, since snowmelt from the cumulative precipitation is a significant part of the streamflow. In the Southwest heavy runoff appears to result from active low mid-latitude storms that tap subtropical Pacific moisture, which is often transported by the subtropical jetstream. This heightened activity occurs over several months from fall through spring, as discussed by Douglas and Englehart [1981], Ropelewski and Halpert [1986], and Andrade and Sellers, [1988]. Increased fall-through-spring precipitation in the Southwest during the El Niño phase of the Southern Oscillation contributes to the observed above normal streamflow. A simplified view of storm tracks and the associated broad scale streamflow anomaly pattern during the mature phase of ENSO is shown in the bottom panel of Figure 9.

Not all basins in this network are well related to PNA, CNP, or SOI. As shown previously in Figure 6, the SLP pattern most reliably correlated with anomalous precipitation and streamflow in California is an SLP anomaly centered to the northwest at about (40" N., 130" W.). The winter 700-mb height teleconnection pattern centered at this origin [see Namias, 1981] shows a similar pattern to the California SLP correlation map. In comparison with the central North Pacific teleconnection the California pattern is more regionally confined, and weakly related to anomalies in the Aleutian Low region. A similar comparison is found for the atmospheric circulation pattern and the regional teleconnection pattern [Namias, 1981] associated with streamflow anomalies along coastal British Columbia. The more regional responses help to explain the lack of a statistical connection between streamflow in these areas and strong or weak atmospheric circulation in the central North Pacific. Said differently, California and British Columbia are close to the node of the atmospheric long wave pattern that emanates from the central North Pacific so that small variations in the

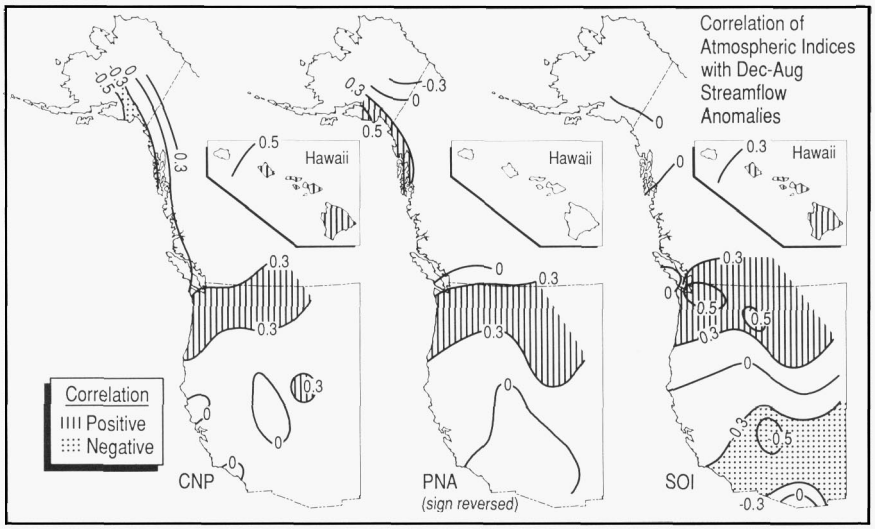

Fig. 8. Correlation between December–August streamflow anomalies and winter CNP (left), PNA (middle) and SOI (right). Sign on PNA was reversed (negative values represent deep Aleutian Low phase) for easier comparison with other indices. Contours at 0, ±0.3, ±0.5.

position of the remote circulation anomaly center can yield either positive or negative streamflow fluctuations.

An ***a posteriori*** perspective of the effect of the atmospheric circulation on streamflow is provided by comparing the annual streamflow at each of four selected rivers with the appropriate area average winter SLP index

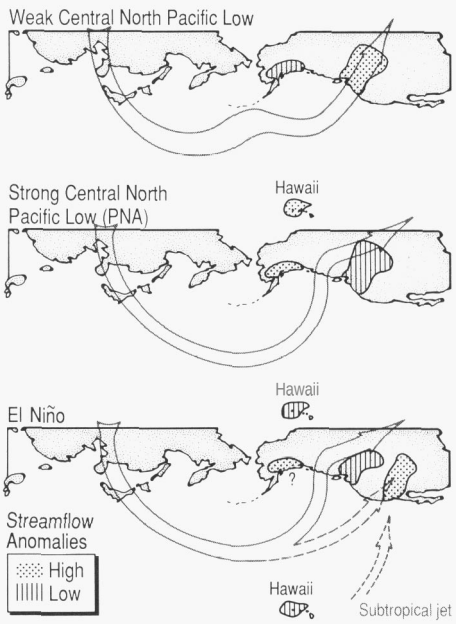

Fig. 9. Schematic of winter atmospheric flow and associated streamflow anomalies during weak central North Pacific low, strong central North Pacific low, and during northern hemisphere winter "mature" phase of El Niño.

(Figure 10). Three of the streams chosen here are taken from the regions that were most sensitive to the central North Pacific low. In addition, an index of winter SLP stationed to the northwest of California centered at (40° N., 130" W.), the region of maximum correlation in Figure 6. This index is founded upon correlations with California precipitation [e.g. Klein and Bloom, 1987] as well as results from this study. The Kenai (coastal Alaska), Clark Fork (Idaho), and Wailua (Hawaii) rivers are each paired to the winter CNP, while the Cosumnes (California Sierra Nevada) is related to winter SLP northwest of the California coast. To emphasize the lower frequency portion of the variability the annual time series have been smoothed with a 1-2-1 weighted running mean filter. The variations in annual streamflow, which are of order 20–40 percent of the climatological mean, are correlated to these SLP indices (winter season only) at the 0.4 to 0.6 level. Many of the major features in the streamflow variability are strongly related to the winter SLP fluctuations. For example, the deficit flow in the Northwest and Hawaii during 1939–1946 was a period of unusually frequent deep winter lows in the central North Pacific (6 of these 8 years have "strong" low winters in Table 2). The relatively high flow in the Northwest between 1948–1957 was a period of weak winter lows in the central North Pacific (7 of these 10 years have "weak" low winters in Table 2). During this period the Pacific Northwest also had generally high precipitation, and snow depth [Walters and Meier, this volume; Ebbesmeyer et. al., this volume]. For Kenai River along the Alaska coast the latter period was one of relatively low streamflow, but there is no streamflow available for the earlier period. Heavy runoff in the California Sierra Nevada during 1978–1983 was a period featuring negative SLP in the eastern North Pacific along the California coast, and scrutiny of time series of Southwest streams plotted in Figure 3 shows that this period stands out as one of the heaviest streamflow episodes in the instrumental record (see also Kay and Diaz [1985] for a discussion of effects of this regime on Great Salt Lake).

Atmospheric Indices Leading Streamflow at Seasonal Time Lags

It is of interest to determine how well streamflow can be predicted from these large scale circulation indices. As a simple first cut at this issue correlations of seasonal SOI, PNA, and CNP versus December–August

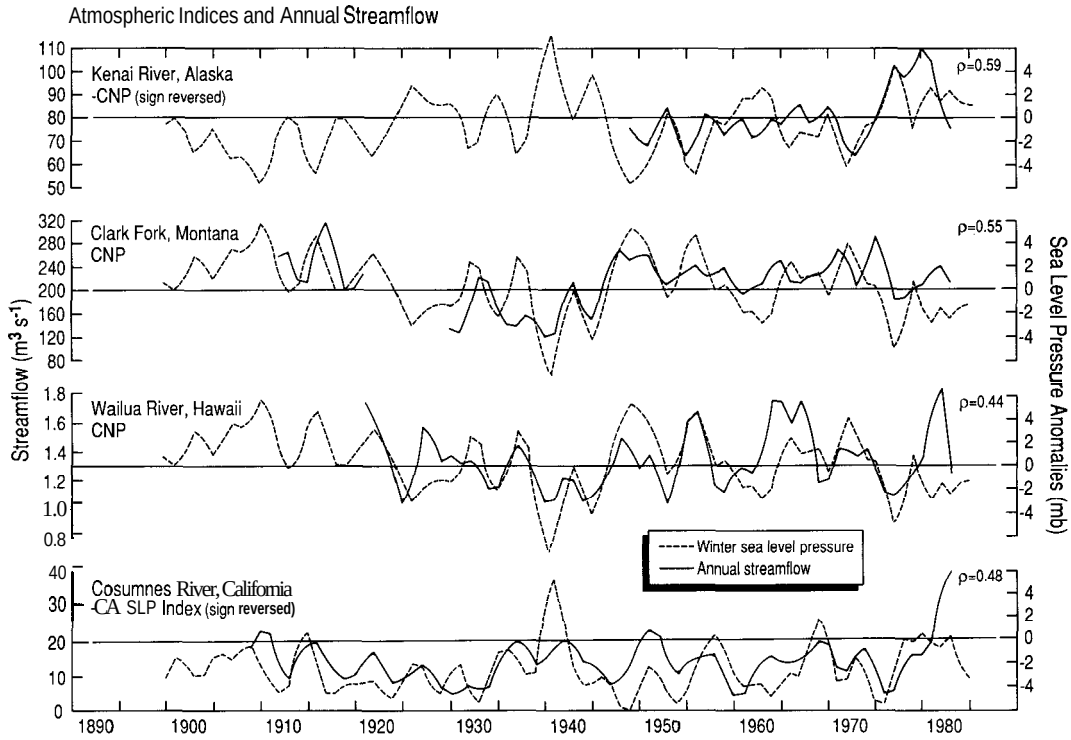

Fig. 10. Annual streamflow and anomalous SLP indices showing relationship to winter CNP for Kenai, Clark Fork, and Wailua Rivers and to SLP anomalies averaged around (40° N., 130" W.) for Cosumnes River. Smoothing by 1-2-1 weighted running mean filter.

streamflow is shown in Table 5. To quantify the effects of seasonal lag relationships, preceding fall (fl-1) PNA and CNP and preceding summer (sm-1) and fall SOI were considered as predictors in addition to winter and spring (during the December–August period) values of all three indices. The active central Pacific period is primarily a cool season phenomenon [Barnston and Livezey, 19871, so summer PNA and CNP predictors were not employed, but SOI is characterized by a time scale of about 1 year (Rasmusson and Carpenter [1982]), so summer SOI was included. Also, lower frequency atmospheric behavior might constitute a better long range predictor, so the average of these indices for two seasons as well as the value for a single season was considered as a single predictor.

The results are encouraging for at least two reasons: (a) predictors preceding the December–August streamflow period account for nearly as much variance as those during winter (the beginning of the streamflow period), and (b) the apparent skill levels, while modest (amount of variance accounted for is 5–25 percent), rivals the skill achieved by state-of-the-artlong range prediction models [Namias, 1980b; Nicholls, 1980]. Predictors from all seasons indicate significant skill for several streams. Spring predictors are generally lower than those from winter. Table 5 shows significant correlations of SOI with streamflow from as early as the previous summer. In fact, summer SOI correlations with December–August streamflow are about the same as those from winter SOI. These results again point out the reliable connection of hydrology in the West to the central North Pacific atmospheric activity that occurs over regionally favored areas. The mechanism leading to the skill at these lags is apparently persistence of the atmospheric circulation, which deploys the North Pacific winter storms as described earlier; the basins that exhibit the strongest correlations with the precursory indices are virtually the same ones that exhibit significant correlations with the winter circulation. The central Pacific Low anomaly is probably among the most predictable northern hemisphere winter circulation features [e.g., Namias, 1985; Dickson and Livezey, 1984]. Barnston and Livezey [1987; Table 4b] have pointed out that there is some tendency of PNA to persist from fall to winter, and ENSO is known to have a high seasonal autocorrelation. More details of long-range predictability using ENSO as a possible predictor are discussed by Madden [1981], Namias and Cayan [1984], and Nicholls [1985]. The change in correlation associated with averaging over two seasons appears to yield modestly higher correlations for fall plus winter CNP, particularly for streams in the northwestern United States; the change in correlations for summer plus fall SOI predictors was insignificant. From this sampling the use of summer SOI or fall SOI individually as predictors is evidently as skillful as using the average of the two. Somewhat surprising is the result that the earlier season predictors, summer SOI and fall PNA, achieved nearly as well as the indices from the season closer to the streamflow period, which would allow for longer forecast leads if it holds up on an independent sample.

Spatial Scales of High versus Low Streamflow

The cross-correlations of streamflow anomalies with atmospheric circulation reveal considerable spatial coherence and suggest possible out-of-phase remote connections of the streamflow anomalies. To quantify the spatial response of anomalous streamflow to its climatic forcings the December–August streamflow anomalies at each individual station were ordered from lowest to highest and years of the lowest and highest extreme

TABLE 5. Cross-Correlation Between Seasonal SOI, PNA, and CNP and Selected Seasonal Streamflow Anomalies

[Correlation coeficients have been multiplied by 100; SM-1, Fl-1 designates summer, fall previous to the December to August streamflow period; W0, Sp0 designates winter, spring during the December to August streamflow period. Winter is December, January, February; spring is March, April, May; summer is June, July, August; fall is September, October, November]

	SOI					PNA					CNP				
	Sm−1	Fl−1	W0	Sp0	Sm−1 + Fl−1	Sm−1	Fl−1	W0	Sp0	Fl−1 + W0	SM−1	Fl−1	W0	Sp0	Fl−1 + W0
Chena River, AK	7	12	19	18	10	31	−27	−18	−26	−24	11	32	24	39	32
Susitna River, AK	12	13	14	2	13	2	−8	−5	−25	−7	26	11	−1	25	4
Kenai River, AK	−19	−23	−26	−21	−21	−13	68	51	6	65	22	−45	−59	−3	−67
Gold Creek, AK	3	−8	−13	−8	−2	12	11	34	10	27	−7	−9	−30	−11	−28
Skeena River, BC	13	15	13	−1	14	−7	−2	−3	−40	−3	1	−9	6	36	2
Fraser River, BC	34	40	39	21	38	8	−14	−22	−49	−21	7	17	26	48	30
Sproat River, BC	−8	−3	0	4	−6	4	−4	14	9	7	13	13	−8	−1	−2
Skagit River, WA	47	53	53	42	51	−3	−23	−36	−29	−36	12	39	37	11	47
Skykomish River, WA	51	57	56	45	55	−9	−31	−44	−27	−45	16	40	41	12	52
Spokane River, WA	36	43	40	33	40	−9	−45	−45	−14	−51	8	41	43	−1	54
Clark River, MT	41	47	44	38	45	−8	−30	−46	−25	−45	−3	35	42	14	51
Clearwater River, ID	44	51	49	38	48	−8	−36	−45	−26	−47	1	39	39	6	50
Yakima River, WA	41	44	36	24	43	−9	−39	−41	4	−46	4	38	38	−9	49
Chehalis River, WA	34	37	34	31	36	−7	−29	−39	−10	−42	12	36	32	−9	43
Wilson River, OR	31	33	30	30	33	−9	−28	−35	−3	−39	5	37	32	−10	43
Willamette River, OR	25	29	28	26	28	−17	−34	−35	0	−41	4	34	38	−13	46
Umpqua River, OR	30	31	27	22	30	−15	−41	−38	−7	−45	−2	35	37	−9	47
John Day River, OR	20	20	14	6	21	−21	−34	−31	4	−37	4	28	25	−23	33
Snake River at Weiser, ID	22	20	17	7	21	−6	−30	−31	24	−35	−13	38	19	−23	32
Snake River near Heise, ID	31	34	36	27	33	−1	−40	−42	13	−46	0	49	32	−6	48
Weber River, UT	6	6	7	16	6	11	−30	−32	17	−35	−9	30	35	−6	42
Yampa River, CO	3	4	2	7	3	14	−39	−17	35	−29	−13	29	17	−27	27
Animas River, CO	−26	−31	−33	−16	−29	8	−15	−16	43	−17	−9	−9	17	−17	12
Green River, UT	−12	−12	−9	2	−12	12	−29	−29	41	−32	−20	16	33	−21	35
Humboldt River, NV	1	−4	−1	2	−2	14	−25	−21	20	−25	−15	31	11	−18	22
Smith River, CA	6	6	3	6	6	−8	−31	−24	5	−32	−11	30	19	−20	29
Sacramento River, CA	−19	−19	−18	−8	−19	3	−23	−10	14	−18	−23	21	2	−26	10
Consumnes River, CA	−13	−15	−16	−3	−14	−3	−26	−22	13	−27	−9	17	16	−27	21
Walker River, CA	−13	−17	−19	−9	−16	5	−24	−20	15	−25	−12	24	14	−21	21
Merced River, CA	−19	−22	−23	−9	−21	2	−27	−19	14	−25	−11	20	12	−24	18
Kings River, CA	−21	−22	−19	−1	−22	5	−17	−18	5	−19	−7	8	12	−16	14
Virgin River, AZ	−50	−56	−58	−32	−54	5	0	−3	48	−2	−11	−14	4	−33	−2
Arroyo Seco, CA	−40	−43	−40	−21	−42	36	3	14	41	11	−19	2	−5	−19	−3
Salt River, AZ	−42	−48	−47	−31	−46	13	−5	2	39	0	−5	−15	5	−5	−1
Gila River, AZ	−46	−51	−48	−27	−49	−1	−14	−6	17	−9	−1	−17	3	−6	−4
San Pedro River, AZ	−13	−7	3	13	−10	−16	6	14	1	12	22	−17	9	−3	1
Wailua River, HI	46	48	50	38	48	1	−22	−52	−59	−45	5	17	55	45	55
Kalihi River HI	24	24	24	26	24	8	20	−27	−20	−9	3	−18	44	15	32

quartiles were identified. Depending on the record length of a given station, the number of cases entering into the low or high quartile ranged from 9 to 20. Composite December–August mean anomalies were constructed for all stations for the years of the (a) low and (b) high quartile of a given station. From maps of the composite the spatial distribution of anomalies associated with low or high streamflow at the given station can be seen. Also, these two composites illustrate whether the spatial pattern of low streamflow anomalies at the given station is different from high streamflow anomalies there. These maps are contoured at 0.5 standard deviation intervals and shaded to indicate significant low or high composite anomalies at the 95 percent confidence level, assuming normally distributed, independent data. In this case significance was estimated using a t-test of the difference between the mean streamflow over the years in the quartile and the mean over the entire sample for that stream (i.e., a test of the null hypothesis). This test was tailored to each station individually due to the varying number of data for different stations.

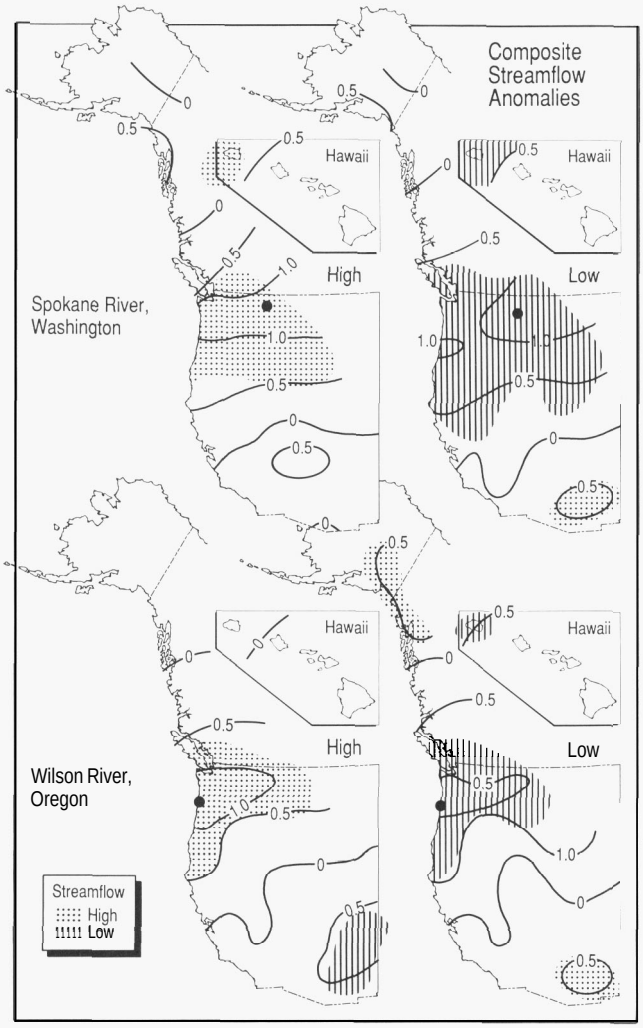

Fig. 11. Composite of December–August streamflow anomalies at all streams for the high (left) and low (right) quartile December–August cases at Spokane (above) and Wilson (below) Rivers. Contours of intervals of 0.5; regions exceeding 95 percent significance level are shaded.

Streams in the Northwest are represented by Wilson River in coastal Oregon and Spokane River in eastern Washington (Figure 11). The composite SLP pattern for high anomalous streamflow at Spokane River (not shown) is similar to the pattern associated with weak atmospheric circulation in the North Pacific, as seen from the CNP, PNA, and SOI. Nearly the opposite pattern is associated with strong circulation over the North Pacific. High streamflow at Spokane River is accompanied by high streamflow at Wailua River in Kauai, and low streamflow along the southern Alaska coast (represented by Gold Creek) and in streams in the Southwest from Southern California through Arizona. Accompanying low streamflow in Spokane River, the low flow in the Northwest extends southward into northern California and Utah, and includes both Hawaiian streams. Although there is a tendency for low streamflow in Spokane River to have associated high streamflow in the Southwest and in coastal Alaska, composite anomalies in these regions do not meet the 95 percent significance level as they did in association with the high flow quartile at Spokane River. For Wilson River the patterns that issue from the heavy and light streamflow anomaly composite are nearly mirror images. High and low streamflow in Wilson River extends eastward to Clark Fork in Montana and southward to Smith River in coastal northern California, and has opposing low and high streamflow anomalies in Arizona. In general, the spatial interrelations of the streamflow variability reflect the patterns established in the precipitation field [see, e.g. Sellers, 1968; McGuirk, 1982].

An interesting difference emerges in the streamflow anomaly composite for California and stations located hundreds of kilometers to the east, which is illustrated by Sacramento River in the California Sierra Nevada and Green River in Utah (Figure 12). The composites derived from these stations show a tendency for negative streamflow anomalies to be more extensive than those for positive streamflow anomalies. From the negative December–August composites for Sacramento River and for Green River the region of 95 percent significant anomalies spans the domain from California to Utah, all of which exceed 0.5 standard deviations. In contrast results for high composites show that positive anomalies of both basins are more confined. Significant positive streamflow anomalies surrounding positive anomalies at Green River are limited to the region eastward of Nevada, while those surrounding positive anomalies at Sacramento River extend from Nevada westward. It is noteworthy that interior basins in the Northwest may show a similar tendency, as low streamflow anomalies at Spokane River (Figure 11) apparently have a larger southward extent than high streamflow anomalies there. At Wilson River, however, no such asymmetries appear.

Does the asymmetry in the streamflow anomaly patterns result from fundamental differences between wet and dry atmospheric circulation regimes? The streamflow anomaly composites imply that atmospheric patterns producing heavy precipitation and high runoff in California are often distinct from ones producing heavy precipitation in Utah and Colorado. On the other hand circulations responsible for extremely dry conditions in California apparently often affect a broader region that extends well into the interior. In fact, there does appear to be prominent contrasts in the respective mean circulation patterns, as revealed by composite SLP anomalies accompanying the positive and negative flow anomalies at Green and Sacramento Rivers in Figure 13. Positive strcamflow anomaly circulations for the Sacramento and Green Rivers are disparate: high streamflow in Sacramento River is associated with negative SLP anomalies centered to the northwest (the characteristic coastal basin pattern discussed previously), and high streamflow in Green River is associated with a broad region of positive SLP anomalies in the central North Pacific centered in the Gulf of Alaska (typical of the interior pattern already discussed). Meanwhile, mean circulations corresponding to low streamflow in the two regions are more similar: both are associated with negative SLP anomalies south of the Aleutian Islands and positive SLP anomalies in the subtropics and to the east along the west coast, although positive anomalies in the eastern Pacific are more strongly developed in the Sacramento River composite.

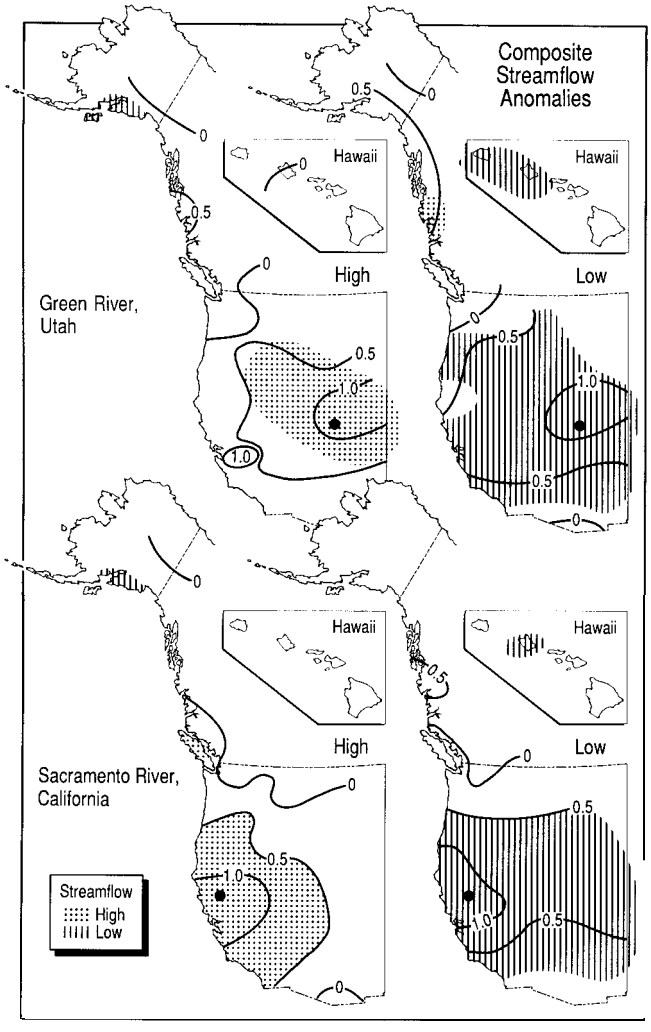

Fig. **12.** Composite of December–August streamflow anomalies at **all** streams for the high (left) and low (right) quartile December–August cases at Green (above) and Sacramento (below) Rivers. Contours of intervals of **0.5;** regions exceeding **95** percent significance level are shaded.

Summary and Conclusions

This study describes aspects of temporal and spatial variability of monthly streamflow in western North America and Hawaii in relation to climate variables. In particular effects of anomalous large scale atmospheric circulation in winter on the resultant streamflow are investigated. Streamflow was represented by **38** streams that cover a large area from Alaska to southwestern United States and also Hawaii. Although this is a sparse array it appears that the ability of streamflow to integrate the spatial and temporal distribution of precipitation within a basin makes this network a useful index of short period climate fluctuations over this broad region. This is particularly important in remote locations with severe terrain and high elevations.

Most of these streams exhibit a strong **annual** cycle. Monthly mean streamflow lags mean precipitation by zero to several months, depending on the climate and probably the physical characteristics of a given basin. The resulting **annual** cycle is not only apparent in the climatological mean streamflow but also pervades most of its other statistics. Compared with precipitation, streamflow is strongly autocorrelated with anomaly time scales ranging between **1** and about **20** months over the **38** stations. Although snow data were not available, cursory examination of the general setting of each particular watershed confirms the well known property that the streamflow persistence is governed by the capacity of a watershed to store precipitation as snow. If the watershed is cold enough (usually this means having high enough elevation), **snowpack** can provide a memory of winter conditions through the runoff season until fall rains begin. During the rising limb of the annual stream hydrograph at the onset of the precipitation season, the relative role of stored water in supporting streamflow declines and, accordingly, the autocorrelation is low. Later, through variations in the timing of the snowmelt, it appears that fluctuations in temperature diminish the autocorrelation. Finally, during the falling limb of the annual stream hydrograph when precipitation has diminished, the relative role of stored water in support of streamflow increases and, therefore, the autocorrelation strengthens.

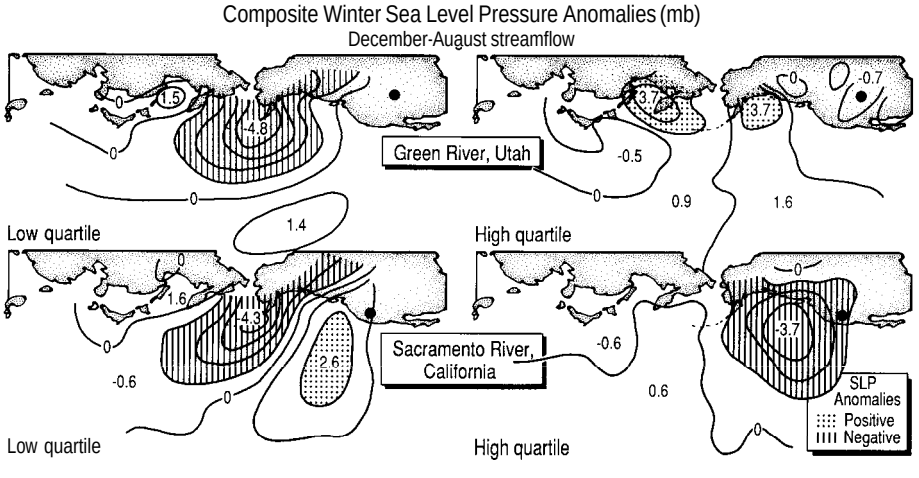

Fig. **13.** Composite winter SLP anomaly (mb) for high (left) and low (right) quartile of December–August cases at Green and Sacramento Rivers; contours at 1 mb intervals; regions with absolute values greater than 1 mb are shaded.

Effects of large scale atmospheric circulation anomalies on streamflow are important enough to be clearly seen despite complications that may be introduced by physical characteristicsof individual watersheds. Topographic controls on the circulation can complicate the pattern of streamflow variability, however, as evidenced by the remarkable lack of correlation between interior and coastal Alaskan streams. Correlation patterns of streamflow with the SLP field were clearest in winter when the atmospheric circulation is most variable and tends to exhibit largest scale anomalies; significant connections to the SLP field were found at all of the basins. In contrast to the contemporaneous relations linking precipitation to the atmospheric circulation, there is a noticeable lag whereby spring-summer streamflow is related to winter SLP in several of the higher elevation or northern basins. This likely results from melting of the snowpack in these watersheds. Because winter SLP-streamflow correlation patterns resemble those relating the mean circulation to precipitation[e.g., Klein and Bloom, 19871, we interpret the connection between winter circulation and streamflow to reflect the precipitation supplied to the watershed via the anomalous storm activity. There are hints that this simple relation linking circulation and precipitation to streamflow breaks down in spring, though, when snowmelt is affected by temperature.

For most basins in the West, SLP grid points having strongest correlations with streamflow were located immediately along the west coast or to west over the ocean, confirming the influence of atmospheric activity over the North Pacific. The pattern of winter atmospheric circulation related to streamflow fluctuations fell into two rather distinct patterns: one for basins near-the-coast and the other for basins in the interior. Both high and low elevation basins near the Pacific coast exhibit connections that tend to be regional in scale, with high streamflow related to negative SLP anomalies to the northwest or the west bringing an active storm track, anomalous southerly to westerly flow, and an ample supply of moist air. In contrast correlations of streamflow basins in the interior west with North Pacific SLP produced teleconnections;e.g., the largest centers are remote rather than local, whereby watersheds from interior Alaska to Utah have increased streamflow in association with anomalously high SLP over the central North Pacific. Because this teleconnection reaches south into the subtropical high, Hawaiian streams are also positively correlated with positive SLP anomalies in the central North Pacific due to enhanced winter trade wind precipitation. Two large scale indices, the well-known PNA index and the CNP, a longer historical surrogate for PNA made from a simple area average of the SLP anomalies south of the Aleutian Islands, represent a major ingredient of these teleconnections. Since atmospheric activity over the central North Pacific tends to be excited during ENSO events, it is not surprising that streamflow is also correlated with the SOI. The spatial patterns of streamflow anomalies associated with SOI resemble those found for precipitation by other investigators(e.g., Douglas and Englehart [1981], Yamal and Diaz [1986], Ropelewski and Halpert [1986], and K. Redmond and R. Koch, personal communication). There is some encouraging evidence that these relations can be used to forecast streamflow anomalies one to two seasons in advance, probably because the associated atmospheric patterns may have large amplitudes and evolve slowly. The SOI seems to have predictive value at least two seasons in advance of the December–August streamflow period (from the previous summer) and the PNA exhibits apparent skill from the preceding fall.

It is important to note that all strong central North Pacific low cases do not have the same precipitation/streamflow patterns over western North America. Similarly, all ENSO cases do not produce the same effects [Namias and Cayan, 1984]. There were marked differences between 1976–1977and 1982–1983, for example, even though both of these winters were El Niño's and had unusually strong North Pacific lows. This is an illustration of how a single area average of the mean circulation is too simplistic to capture variations from one case to the next or between regions. A better specification of precipitation and streamflow could be made by accounting for the longitudinal position of the low, which is related to the meridional component of the geostrophic flow anomaly. Some regions in the West are not statistically well related to the central North Pacific circulation mode. Regionally, we found no significant correlations with either PNA or SOI for streamflow in interior Alaska, British Columbia, California, and Nevada. These regions lie between the strong centers of activity of the strong central North Pacific teleconnection pattern, and streamflow anomalies in these regions are strongly correlated with other regional atmospheric patterns.

The large scale of atmospheric circulation anomalies is reflected in the spatial pattern of streamflow anomalies. While streamflow is high/low in southern Alaska and northern British Columbia, it tends to be low/high in streams in California eastward through Colorado. Similarly, when streams have high/low flow in the Pacific Northwest, those in Arizona are often low/high. These patterns seem consistent with results of previous studies [e.g., Langbein and Slack, 1982; Meko and Stockton, 1984; Lins, 1985] of streamflow from different station arrays that covered part of the domain considered here. There appears to be an asymmetry in the east–west extent of dry, as opposed to wet, streamflow regimes in the California-through-Colorado region. Comparison of low and high quartiles of streamflow cases from the available record shows that while low streamflow in the Southwest often includes a broad region from California eastward to Colorado, the high flow cases for California were more confined to the far west. High flows in Colorado and Utah are usually clustered in the southern Rockies and not as strongly to the west. There was a hint that the spatial scale of low streamflow in the interior northwest also tends to be larger than that for high flow. These anomaly pattern differences appear to result from an asymetry in the circulations causing low versus high precipitation. This nonlinear behavior, if real, is noteworthy because of the different scales implied for drought versus wet conditions in the Southwest.

Perhaps the greatest social and economic impacts of these fluctuations result from periods of prolonged high or low streamflow, and it is important to view modern day variations in the context of the fluctuations over the entire available record. During the earlier part of the record can be seen a persistent episode of the unusually high streamflow throughout the Southwest during the early 1900's (e.g., see Weber River anomaly plot in Figure 3), while prolonged low flows show up in all streams in the northwestern United States during the mid-1920's through the early 1940's. The CNP index provides a simple means of analysis and interpretation of regional climate variability influenced by the North Pacific atmospheric teleconnection and is well related to low and high streamflow episodes at sensitive regions in this domain. Large spatial variations can also be interpreted from the point of view of the North Pacific circulation. Interestingly, the out-of-phase tendency between coastal Alaskan streams and those in the Pacific Northwest are similar to behavior of the mass balances of glaciers in these same regions [Walters and Meier, this volume]. Other physical and biological systems in the region show the influence of these decadal climatic variations [e.g., Ebbessmeyer et. al., this volume; Venrick et. al., 1987]. Also, although this study has focused on western North America and Hawaii, previous work [e.g., Ropelewski and Halpert, 19861 has demonstrated that large scale atmospheric modes such as ENSO are connected to precipitation farther downstream east of the Rockies, and it seems likely that the remainder of the North America streamflow link to North Pacific atmospheric forcing will emerge in a similar analysis over a larger stream network.

Acknowledgments. Discussions with Nick Graham, Art Douglas, Roy Walters, Tony Barnston, Sue Ann Bowling, and Chet Ropelewski were very useful, as were comments by Bill Klein, Henry Diaz, Jerome Namias, Dave Meko, and two anonymous reviewers. Careful editing and suggestions by Jurate Landwehr improved the manuscript significantly. We also thank Tom Ross of the U.S. Geological Survey for streamflow anomaly maps. Much credit goes to Ray Herndon for data processing, Emelia Bainto and Tam Vu for calculations, computer plotting and editing, and to Marguerette Schultz and Jeanne DiLeo-Stevens for excellent artwork. Mary Ray and Martha Nichols prepared illustrations and tables, provided expert editorial help, and skillfully processed several versions of the manuscript.

DRC greatly appreciates funding for this work from the National Climate Program Office through the Experimental Climate Forecast Center program, Grant NA86-AA-D-CP104; National Science Foundation, Grant ATM86-12853; the United States Geological Survey, Grant 14-08-0001-G1483; the University of California Water Resources Center, Project Number W-720; and through the University of California INCOR Program between Scripps Institution of Oceanography, Lawrence Livermore National Laboratory, and Los Alamos National Laboratory. The authors also thank the U.S. Geological Survey, National Science Foundation, the National Climate Program Office, and the Monterey Bay Aquarium for funding the PACLIM Workshop Series, where ideas for this work originated.

References

Andrade, E. R., and Sellers, W. D., El Nifio and its effect on precipitation in Arizona and western New Mexico, ***Journal of Climatology,*** p. 403–410, 1988.

Barnston, A. G., and Livezey, R. E., Classification, seasonality and persistence of low-frequency atmospheric circulation patterns, ***Monthly Weather Review,*** v. 115, p. 1083–1126, 1987.

Bartlein, P. J., Streamflow anomaly patterns in the U.S.A. and southern Canada 1951–1970, ***Journal of Hydrology,*** v. 57, p. 49–63, 1982.

Blackmon, M. L., Lee, Y.-H., Wallace, J. M., and Hsu, H.-H., Time variation of 500 mb height fluctuations with long, intermediate and short time scales as deduced from lag-correlation statistics, ***Journal of Atmospheric Science,*** v. 41, p. 981–991, 1984.

Bjerknes, J., Atmospheric teleconnections from the equatorial Pacific, ***Monthly Weather Review,*** v. 97, p. 163–172, 1969.

Cayan, D. R., and Roads, J. O., Local relationships between United States west coast precipitation and monthly mean circulation parameters, ***Monthly Weather Review,*** v. 112, p. 1276–1282, 1984.

Cayan, D. R., Ropelewski, C. F., and Karl, T. R., ***An Atlas of United States Monthly and Seasonal Temperature Anomalies, December 1930–November 1984,*** Published by the NOAA National Climate Program Office, Rockville, MD, p. 244, 1986.

Court, A., Water balance estimates for the United States, ***Weatherwise,*** v. 27, p. 252–259, 1974.

Davis, R. E., Predictability of sea level pressure anomalies over the North Pacific Ocean, ***Journal of Physical Oceanography,*** v. 8, p. 233–246, 1978.

Department of the Interior, Index stations and selected large-river streamgaging stations in the west, p. 11, ***Water Resources Review,*** U.S. Geological Survey, April 1975.

Diaz, H. F., Areally-weighted temperature and precipitation for Alaska, 1931–1977, ***Monthly Weather Review,*** v. 108, p. 817–822, 1980.

Dickson, R. R., and Livezey, R. E., On the contribution of major warming episodes in the tropical East Pacific to a useful prognostic relationship based on the Southern Oscillation, ***Journal of Climate and Applied Meteorology,*** v. 23, p. 194–200, 1984.

Douglas, A. V., Cayan, D. R., and Namias, J., Large-scale changes in North Pacific and North American weather patterns in recent decades, ***Monthly Weather Review,*** v. 110, p. 1852–1862, 1982.

Douglas, A. V., and Englehart, P. J., On a statistical relationship between rainfall in the central equatorial Pacific and subsequent winter precipitation in Florida, ***Monthly Weather Review,*** v. 109, p. 2377–2382, 1981.

Ebbesmeyer, C. C., Coomes, C. A., Cannon, G. A., and Bretschneider, D. E., Linkage of ocean and fjord dynamics at decadal period in ***Aspects of Climate Variability in the Pacific and the Western Americas,*** edited by D. H. Peterson, American Geophysical Union, Washington, DC, this volume, 1989.

Esbensen, S. K., A comparison of intermonthly and interannual teleconnections in the 700 mb geopotential height field during the northern hemisphere winter, ***Monthly Weather Review,*** v. 112, p. 2016–2032, 1984.

Emery, W. J., and Hamilton, K., Atmospheric forcing of interannual variability in the northeast Pacific Ocean: Connections with El Nifio, ***Journal of Geophysical Research,*** v. 90, p. 857–868, 1985.

Fu, C., Diaz, H. F., and Fletcher, J. O., Characteristics of the response of sea-surface temperature in the central Pacific associated with warm episodes of the Southern Oscillation, ***Monthly Weather Review,*** v. 114, p. 1716–1738, 1986.

Granger, O. E., Secular fluctuations of seasonal precipitation in lowland California, ***Monthly Weather Review,*** v. 105, p. 386–397, 1977.

Holmes, S. L., Monthly streamflow and ground-water conditions in the United States and southern Canada, water years 1945–85, Department of the Interior, ***U.S. Geological Survey Water-Supply Paper 2314,*** p. 250, 1987.

Horel, J. D., and Wallace, J. M., Planetary scale atmospheric phenomena associated with the Southern Oscillation, ***Monthly Weather Review,*** v. 109, 813–829, 1981.

Hsu, C. F., and Wallace, J. M., The global distribution of the annual and semiannual cycles in precipitation, ***Monthly Weather Review,*** v. 104, p. 1093–1101, 1976.

Jones, P. D., The early twentieth century Arctic high - fact or fiction? ***Climate Dynamics,*** v. 1, p. 63–75, 1987.

Kay, P. A., and Diaz, H. F. (editors), ***Problems and Prospects for Predicting Great Salt Lake Levels,*** p. 308, papers presented at a conference held in Salt Lake City, March 26–28, 1985, Center for Public Affairs and Administration, University of Utah, 1985.

Karl, T. R., and Knight, R. W., ***Atlas of Monthly and Seasonal Precipitation Departures from Normal (1895–1985) for the Contiguous United States,*** Historical Climatology Series 3–12, p. 213, National Climatic Data Center, Asheville, NC, 1985.

Klein, W. H., Principal tracks and mean frequencies of cyclones and anticyclones in the northern hemisphere, ***Research Paper*** No. ***40,*** U.S. Weather Bureau, Washington, DC, p. 60, 1957.

Klein, W. H., Specification of precipitation from the 700-millibar circulation, ***Monthly Weather Review,*** v. 91, p. 527–536, 1963.

Klein, W. H., Crockett, C. W., and Andrews, J. F., Objective prediction of daily precipitation and cloudiness, ***Journal of Geophysical Research,*** v. 70, p. 801–813, 1965.

Klein, W. H., and Bloom, H. J., Specification of monthly precipitation over the United States from the surrounding 700 mb height field, ***Monthly Weather Review,*** v. 115, p. 2118–2132, 1987.

Langbein, W. B., and Slack, J. R., Yearly variations in runoff and frequency of dry years for the conterminous United States, 1911–79, ***U.S. Geological Survey Open-File Report 82-751,*** 85 p., 1982.

Leith, C. E., The standard error of time-average estimates of climatic means, ***Journal of Applied Meteorology,*** v. 12, p. 1066–1069, 1973.

Lins, H. F., Streamflow variability in the United States: 1931–1978, Journal of Climate and Applied Meteorology, v. 29, p. 463–471, 1985.

Livezey, R. E., and Mo, K. C., Tropical-extratropical teleconnections during the northern hemisphere winter, Part II: Relationships between monthly mean northern hemisphere circulation patterns and proxies for tropical convection, ***Monthly Weather Review,*** v. 115, p. 3115–3132, 1987.

Lyons, S. W., Empirical orthogonal function analysis of Hawaiian rainfall, ***Journal of Applied Meteorology,*** v. 21, p. 1713–1729, 1982.

Madden, R. A., Observations of large-scale traveling Rossby waves, ***Reviews of Geophysics and Space Physics,*** v. 17, p. 1935–1949, 1979.

Madden, R. A., A quantitative approach to long-range prediction, ***Journal of Geophysical Research,*** v. 86, p. 9817–9825, 1981.

McGuirk, J. P., A century of precipitation variability along the west coast of North America and its impact, ***Climatic Change,*** v. 4, p. 41, 1982.

Meko, D. M., and Stockton, C. W., Secular variations in streamflow in the western United States, *Journal of Climate and Applied Meteorology*, v. **23**, p. **889–897, 1984.**

Moss, M. E., and Bryson, M. C., Autocorrelation structure of monthly streamflows, *Water Resources Research*, v. **10**, p. **737–744, 1974.**

Namias, J., Northern hemisphere seasonal sea level pressure and anomaly charts, **1947–1974**, *CalCOFI Atlas No. 22*, edited by **A.** Fleminger, Marine Life Research Program, Scripps Institution of Oceanography, University of California-San Diego, La Jolla, CA, p. **243, 1975.**

Namias, J., Multiple causes of the North American abnormal winter **1976–77**, *Monthly Weather Review*, v. **106**, p. **279–295, 1978a.**

Namias, J., Persistence of U.S. seasonal temperatures up to one year, *Monthly Weather Review*, v. **106**, p. **1557–1567, 1978b.**

Namias, J., The art and science of long-range forecasting, *EOS*, v. **60**, p. **449–450, 1980.**

Namias, J., Teleconnections of **700** mb height anomalies for the northern hemisphere, *CalCOFI Atlas No.* 29, p. **265**, Fleminger, Marine Life Research Program, Scripps Institution of Oceanography, University of California-San Diego, La Jolla, CA, **1981.**

Namias, J., New evidence for relationships between North Pacific atmospheric circulation and El Niño, *Tropical Ocean-Atmosphere Newsletter*, March **1985**, p. **2–3, 1985.**

Namias, J., and Cayan, D. R., El Niño implications for forecasting, *Oceanus*, v. **27**, p. **41–47, 1984.**

Namias, J., Yuan, X., and Cayan, D. R., Persistence of North Pacific sea surface temperature and atmospheric flow patterns, *Journal of Climate*, v. **1**, p. **682–703, 1988.**

Nicholls, N., Towards the prediction of major Australian droughts, *Australian Meteorology Magazine*, p. **33**, p. **161–166, 1985.**

Nicholls, N., Long-range weather forecasting value, status, and prospects, *Review of Geophysics and Space Physics*, v. **18**, p. **771–788, 1980.**

Peterson, D. H., Cayan, D. R., Dileo-Stevens, J., and Ross, T. G., Some effects of climate variability on hydrology in western North America: The Influence of Climate Change and Climatic Variability on the Hydrologic Regime and Water Resources, *Proceedings of the Vancouver Symposium, August 1987, IAHS Publication no. 168*, 1987a.

Peterson, D. H., Hager, S. W., Schemel, L. E., and Cayan, D. R., Riverine C, N, Si, and P transport to the coastal ocean: An overview, in *Coastal-Offshore Ecosystem Interactions*, Lecture Notes on Coastal and Estuarine Studies, edited by B. **O.** Jansson, v. **22**, p. **227–253**, Springer-Verlag, Berlin, **1987b.**

Peterson, D. H., Cayan, D. R., and Festa, J. F., Interannual variability in biogeochemistry of partially mixed estuaries dissolved silicate cycles in northern San Francisco Bay, in *Esuarine Variability*, edited by D. A. Wolfe, p. 123–138, Academic Press, New York, 1986.

Pittock, A. B., On the causes of local climatic anomalies, with special reference to precipitation in Washington state, *Journal of Applied Meteorology*, v. **16**, p. **223–230, 1977.**

Pyke, C. B., Some meteorological aspects of the seasonal distribution of precipitation in the western United States and Baja, California, Contribution No. **139** (UCAL–WCR–W–254), p. **205**, University of California, Water Resources Center, Los Angeles, CA, **1972.**

Quinn, W. H., and Neal, V. T., El Niño occurrences over the past four and a half centuries, *Journal of Geophysical Research*, v. **92**, p. 14449–14461, **1986.**

Quiroz, R. **S.**, The climate of the El Niño winter of **1982–1983:** A season of extraordinary climatic anomalies, *Monthly Weather Review*, v. 111, p. **1685–1706, 1983.**

Rasmusson, E. M., Atmospheric water vapor transport and the water balance of North America, Part **1.** Characteristics of the water vapor flux field, *Monthly Weather Review*, v. **95**, p. 403–426, **1967.**

Rasmusson, **E.** M., and Carpenter, T. H., Variations in tropical sea surface temperature and surface wind fields associated with the Southern Oscillation/El Niño, *Monthly Weather Review*, v. **110**, p. **354–384, 1982.**

Reitan, C. H., Frequencies of cyclones and cylogenesis for North America, **1951–1970**, *Monthly Weather Review*, v. **102**, p. **861–868, 1974.**

Roden, **G., On** river discharge into the northeastern Pacific Ocean and the Bering Sea, *Journal of Geophysical Research*, v. **72**, p. **5613–5629, 1967.**

Ropelewski, C. F., and Halpert, M. S., North American precipitation and temperature patterns associated with the El Niño/Southern Oscillation (ENSO), *Monthly Weather Review*, v. **114**, p. **2352–2362, 1986.**

Sellers, W. D., *Physical Climatology*, p. **272**, University of Chicago Press, Chicago, IL, **1965.**

Sellers, W. D., Climatology of monthly precipitation patterns in western United States, *Monthly Weather Review*, v. **96**, p. **585–595, 1968.**

Solot, **S.** B., Further studies in Hawaiian precipitation, *Research Paper No. 32*, p. **37**, U.S. Weather Bureau, Washington, DC, **1950.**

State of California, *California Water Atlas*, edited by W. L. Kharl, p. **118, 1979.**

Stidd, C. K., The use of correlation fields in relating precipitation to circulation, *Journal of Meteorology*, v. **11**, p. **202–213, 1954.**

Trenberth, **K.** E., and Paolino, D. A., The northern hemisphere sea-level pressure data set trends, errors, and discontinuities, *Monthly Weather Review*, v. **108**, p. **855–872, 1980.**

Venrick, E. L., McGowan, J. **A.**, Cayan, D. R., and Hayward, T. L., Climate and chlorophyll a long-term trends in the central North Pacific Ocean, *Science*, v. **238**, p. **70–72, 1987.**

Wallace, J. M., and Gutzler, D. S., Teleconnections in the geopotential height field during northern hemisphere winter, *Monthly Weather Review*, v. **109**, p. **784–812, 1981.**

Walsh, J. E., Richman, M. B., and Allen, D. W., Spatial coherence of monthly precipitation in the United States, *Monthly Weather Review*, v. **110**, p. **272–286, 1982.**

Walters, R., and Meier, M. F., Variability of glacier mass balances in western North America, in *Aspects of Climate Variability in the Pacific and the Western Americas*, edited by D. H. Peterson, this volume, American Geophysical Union, Washington, DC, **1989.**

Weare, B. C., and Hoeschele, M. A., Specification of monthly precipitation in the western United States from monthly mean circulation, *Journal of Climate and Applied Meteorology*, v. **22**, p. **1000–1007, 1983.**

Weaver, R. C., Meteorology of hydrological critical storms in California, *Hydrometeorological Report* No. *37*, p. **207**, U.S. Department of Commerce, Weather Bureau, Washington, DC, **1962.**

Yamal, B., and Diaz, H. F., Relationships between extremes of the Southern Oscillation and the winter climate of the Anglo-American Pacific Coast, *Journal of Climate*, v. **6**, p. **197–219, 1986.**